Clim. Past, 22, 205–226, 2026
https://doi.org/10.5194/cp-22-205-2026

Climate of the Past
Open Access
EGU

A global analysis of pollen-based reconstructions of land climate changes during Dansgaard–Oeschger events

Mengmeng Liu[1,2], **Iain Colin Prentice**[1], **and Sandy P. Harrison**[2]

[1]Georgina Mace Centre for the Living Planet, Department of Life Sciences, Imperial College London, Silwood Park Campus, Buckhurst Road, Ascot SL5 7PY, UK
[2]Department of Geography and Environmental Science, University of Reading, Reading, RG6 6AB, UK

Correspondence: Mengmeng Liu (m.liu18@imperial.ac.uk)

Received: 24 February 2024 – Discussion started: 12 March 2024
Revised: 20 November 2025 – Accepted: 8 January 2026 – Published: 2 February 2026

Abstract. Dansgaard–Oeschger (D–O) warming events are comparable in magnitude and rate to the anticipated 21st century warming. As such, they provide a good target for evaluation of the ability of state-of-the-art climate models to simulate rapid climate changes. Despite the wealth of qualitative information about climate changes during the D–O events, there has been no attempt to date to make quantitative reconstructions globally. Here we use frequency-corrected Tolerance-weighted Weighted Averaging Partial Least Squares regression (*fx*TWA-PLS) to reconstruct mean temperature of the coldest month, mean temperature of the warmest month, and a plant-available moisture index across multiple D–O events between 50 and 30 ka based on available pollen records across the globe. The reconstruction of plant-available moisture is corrected for the impact of changing atmospheric CO_2 concentrations on plant water use efficiency. These reconstructions show that the largest warming occurred in northern extratropics, especially Eurasia, while western North America and the southern extratropics were characterised by cooling. The change in winter temperature was significantly larger than the change in summer temperature in the northern extratropics and the tropics, indicating that the D–O warming events were characterised by reduced seasonality, but there was no significant difference between the summer and winter temperature changes in the southern extratropics. The antiphasing between northern and southern extratropical changes, and the west-east pattern of cooling and warming in North America were generally consistent across the eight D–O events examined, although coherency is greatest during the strongest events. There was no globally consistent pattern between changes in moisture and changes in temperature. These reconstructions can be used to evaluate the spatial patterns of changes in temperature and moisture in the transient simulations of the D–O events planned as part of the Palaeoclimate Modelling Intercomparison Project.

1 Introduction

Dansgaard–Oeschger (D–O) events are characterised in Greenland by a transition from cold Greenland Stadial (GS) to warmer Greenland Interstadial (GI) conditions (Dansgaard et al., 1993). The surface air temperature in Greenland increased by 10–16 °C during the warming phases; these warming events occurred over an interval of between 50 and 200 years (Huber et al., 2006; Kindler et al., 2014). Thus, the D–O events offer a parallel in terms of speed to projected future warming, although both the baseline state and the mechanism inducing this warming differ from anticipated 21st century climate changes. D–O events could therefore provide an opportunity to determine how well climate models that are used for future projections can simulate rapid climate changes (Malmierca-Vallet et al., 2023), particularly regional patterns of warming (and cooling) that are regarded as a challenge for modelling (Doblas-Reyes et al., 2021; Lee et al., 2021) and are highly important in assessing the vulnerability of human societies to future climate changes (IPCC, 2022).

Although D–O events are found throughout the last glacial period, the largest number and the most regular patterning occurred during Marine Isotope Stage 3 (MIS 3; 57 to 29 ka) when there were 11 separate events (D–O 15 to D–O 5),

while MIS 4 (71 to 57 ka) only had 3 separate events (D–O 18 to 16) (Kindler et al., 2014). The typical duration of a cycle as manifested in Greenland is ca. 1500 years and is characterised by an initial short slow warming, followed by an abrupt large warming in matter of decades, followed by a long slow cooling over centuries to millennia, with a terminal phase of fast cooling (e.g. D–O 8, D–O 12); however, there are also cycles in which the warming and cooling phases took roughly the same time (e.g. D–O 5, D–O 6, D–O 9) (Kindler et al., 2014). The magnitude of changes also differ, with both strong events (e.g. D–O 8, D–O 12) and weak events (e.g. D–O 9) (Kindler et al., 2014).

The D–O signals are not just seen in Greenland – they are registered globally (Adolphi et al., 2018; Corrick et al., 2020; Harrison and Sanchez Goñi, 2010; Sánchez Goñi et al., 2017; Voelker, 2002) and are reflected in changes in both temperature and precipitation. Both oceanic and ice-core records indicate that temperature changes are out-of-phase between the northern and southern hemispheres, and the southern hemisphere response both in terms of warming and cooling phases is generally less abrupt (Dima et al., 2018; Vettoretti and Peltier, 2015). There is a comparative lack of information from the continents about the manifestation of D–O events. Shifts in vegetation types between GI and GS states have been interpreted as primarily a temperature signal in the extratropics and a moisture signal in the tropics (Harrison and Sanchez Goñi, 2010). Speleothem records provide a good time-control on the synchroneity of climate changes globally with the D–O events registered in Greenland (Adolphi et al., 2018; Corrick et al., 2020), but the driver of this signal can either be temperature or precipitation depending on the region. There are quantitative climate reconstructions based on terrestrial pollen records from La Grande Pile (Guiot et al., 1993), Lago Grande di Monticchio (Huntley et al., 1999), Padul (Camuera et al., 2022), El Cañizar de Villarquemado (Camuera et al., 2022; Wei et al., 2021) and Lake Ohrid (Sinopoli et al., 2019), marine cores in the western Mediterranean and offshore from Portugal (Sánchez Goñi et al., 2002), diatom assemblages at Les Echets, France (Ampel et al., 2010), chironomids from Lake Bergsee in central Europe (Lapellegerie et al., 2024), bacterial membrane lipid records from the Eifel region (Zander et al., 2024), isotopic measurements of earthworm calcite from the Rhine Valley (Prud'homme et al., 2022) and clumped isotope measurements on snails in Hungary (Újvári et al., 2021). Aside from the lack of comparable quantitative estimates from outside Europe, differences in the methodology employed and in the specific climate variables reconstructed in each of these studies limits their usefulness for model evaluation. In particular, given that there is still uncertainty as to whether the D–O cycles are characterised by changes in seasonality such that warming events are primarily driven by changes in winter (Flückiger et al., 2008; Zander et al., 2024; Zumaque et al., 2025), in the regional strength of the warming (Harrison and Sanchez Goñi, 2010) and how warming relates to changes in moisture (Wei et al., 2021), there is a need for more systematic reconstruction of seasonal climate changes.

In the paper, we provide reconstructed changes in seasonal temperatures and plant-available moisture during the intervals corresponding to D–O warming events in Greenland between 50 and 30 ka based on available pollen records globally, using a standard regression-based approach, *fx*-corrected Tolerance-weighted Weighted Averaging Partial Least Squares (*fx*TWA-PLS: Liu et al., 2020, 2023). We also correct the reconstructions of plant-available moisture to take account of the impact of lower CO_2 on plant water-use efficiency following Prentice et al. (2022a). We analyse the regional patterns to identify key targets for model evaluation.

2 Methods

2.1 Data sources

2.1.1 Modern pollen dataset

Modern pollen data were obtained from version 3 of the SPECIAL Modern Pollen Dataset (SMPDSv3) (Harrison et al., 2025a). This global dataset was constructed by amalgamating and standardising records from public repositories (e.g. Neotoma, Pangaea), existing regional databases (e.g. European Modern Pollen Database, African Pollen Database), individual publications and records provided by the original authors. The records were carefully screened to remove duplicates that were present in more than one source. The modern samples were obtained from multiple types of record, including pollen traps, surface samples, moss polsters and different types of sediment, including cores from lakes and peatbogs, and section through e.g. fluvial or loess deposits. In cases where the record was radiometrically dated, the database preserves all samples younger than 50 yr BP. However, some samples were undated and are therefore recorded as modern if a collection date was given or assumed modern if not.

The dataset contains 26 704 samples from 18 202 different locations, and was created after removing taxa that are not climatically diagnostic (e.g. obligate aquatics, carnivorous species, cultivated plants). The dataset provides several levels of taxonomic aggregation; here we use the most aggregated level, where woody species were generally combined at genus level and herbaceous species at sub-family or family level unless they were palynologically distinctive, occupied distinctive ecological niches and were sufficiently geographically widespread. This "amalgamated" dataset contains relative abundance information for 1367 taxa. These samples were aggregated by location (longitude, latitude and elevation) in order to remove duplicates. Counts for *Quercus*, *Quercus* (deciduous) and *Quercus* (evergreen) were combined because of inconsistent differentiation of *Quercus* pollen in different regional records. Deciduous and evergreen oaks occupy different areas of climate space, partic-

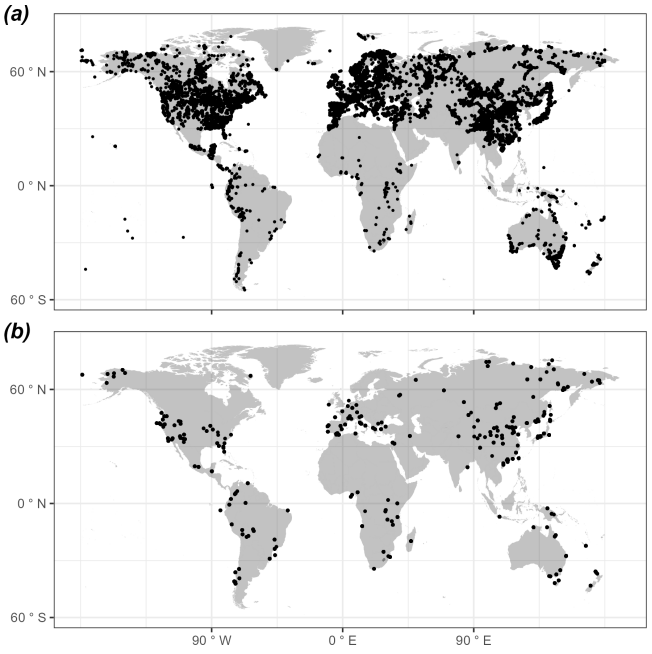

Figure 1. Map showing the locations of **(a)** modern pollen records used to derive the pollen-climate transfer functions, and **(b)** fossil pollen records covering the interval 50–30 ka used for the climate reconstructions.

ularly in terms of seasonal moisture; specifically, evergreen oaks are typically found in areas characterised by winter rainfall such as the Mediterranean. Nevertheless, since there are other plant taxa that are similarly diagnostic of such regimes, the amalgamation of *Quercus* (deciduous) and *Quercus* (evergreen) should not have a major effect on the robustness of our climate reconstructions. We have tested this assumption by making reconstructions based on all taxa except *Quercus* (Supplement, Sect. S4). Taxa that occurred in less than 10 samples in the training dataset were not used to make reconstructions because it is unlikely that the available samples provided a reasonable estimate of the climate space occupied by these rare taxa (Liu et al., 2020). After the location aggregation and the taxa filter, the dataset contains information on 18 202 samples with relative abundance information for 609 taxa (Fig. 1a).

We focus on three climate variables: mean temperature of the coldest month (MTCO), mean temperature of the warmest month (MTWA), and a plant-available moisture index (α_{plant}) defined as the estimated ratio of actual to equilibrium evapotranspiration. These three variables reflect ecophysiological controls on plant distribution (Harrison, 2020; Woodward, 1987) that have been shown to independently influence the distribution and abundance of plant species (Boucher-Lalonde et al., 2012; Wang et al., 2013; Wei et al., 2020). α_{plant} is a transformation of the commonly used moisture index MI (defined as the estimated ratio of annual precipitation to annual potential evapotranspiration) that emphasizes differences at the dry end of the climate range, which have a more pronounced effect on vegetation distribution than differences at the wet end (Prentice et al., 2017). Thus, α_{plant} can be better reconstructed from the pollen records than MI.

The climate values at each SMPDSv3 site were obtained using a geographically-weighted regression (GWR) of climatological values of mean monthly temperature, precipitation, and fractional sunshine hours from the Climatic Research Unit Time-Series version 4.04 (CRU TS4.04; Harris et al., 2020) dataset averaged over the period 1961–1990, which corresponds to the interval from which most of the pollen samples were derived. GWR was to correct for elevation differences between the CRU grid cells and the pollen sites. MTCO and MTWA were taken directly from the GWR. MI was calculated for each site using SPLASH v1.0 (Davis et al., 2017) based on daily values of precipitation, temperature and sunshine hours obtained using a mean-conserving interpolation of the monthly values of each. MI was then transformed to α_{plant} using the parametric Fu-Zhang formulation of the Budyko relationship (Supplement, Sect. S2). The climate space occupied by SMPDSv3 (Fig. S1 in the Supplement) samples a reasonable range of global climate space and therefore should provide robust reconstructions of climate changes under glacial conditions.

We use a global modern dataset for calibration of the pollen-climate relationships. The use of a global dataset, rather than region-specific training data, relies on the principle of phylogenetic niche conservatism (Harvey and Pagel, 1991; Qian and Ricklefs, 2004; Wang et al., 2025), which states that traits tend to remain constant over time and that the climatic niches of specific genera are also conservative (Harrison et al., 2025c). The use of a global dataset for calibration makes it possible to sample a large range of climates, and thus makes it more likely that the reconstructions of glacial climates are realistic and not confined to the limited climate range sampled in any one region in modern times (Turner et al., 2020).

2.1.2 Fossil pollen dataset

The Abrupt Climate Changes and Environmental Responses (ACER) database (Sánchez Goñi et al., 2017) was originally created to provide a source of pollen and charcoal data for Marine Isotope Stage 3 (MIS 3), which includes 93 records with sufficient resolution and dating control to detect sub-millennial scale variability. Many more records covering MIS 3 have become available since the compilation of the ACER database, such as the synthetic pollen databases available for Siberia (Cao et al., 2019, 2020) and China (Zhou et al., 2023) and the global Legacy 2 dataset (Li et al., 2025), which can substantially cover the spatial gaps in the original ACER database. We obtained these data from public sources or directly from the authors and used them to create an update: ACER2 (Harrison et al., 2025b), which contains 233

additional records covering some part or all of MIS 3 (note that the original ACER records are not included in ACER2 due to licensing issue). The two datasets are combined in our analyses to serve as the fossil pollen dataset (Supplement, Sect. S3) to reconstruct the past climates. We focus on the 279 records (253 terrestrial records and 26 marine records) between 50 and 30 ka (Fig. 1b; Table 1). The fossil pollen data are taxonomically harmonised to be consistent with the SMPDSv3.

2.2 Climate reconstruction method

We use *fx*-corrected Tolerance-weighted Weighted Averaging Partial Least Squares (*fx*TWA-PLS: Liu et al., 2020, 2023) regression to derive the pollen-climate relationships in the modern training dataset, and then apply these relationships to reconstruct past climates from the fossil pollen records (Fig. 2). *fx*TWA-PLS reduces the tendency of regression methods to compress reconstructions towards the centre of the sampled climate range by applying a sampling frequency correction to reduce the influence of uneven sampling of climate space and weighting the contribution of individual taxa according to their climate tolerances (Liu et al., 2020). Version 2 of *fx*TWA-PLS (*fx*TWA-PLSv2: Liu et al., 2023) uses P-splines smoothing to derive the frequency correction and applies this correction both in estimating the climate optima and tolerances, and in the regression itself, producing a further improvement in model performance compared to *fx*TWA-PLSv1 (Liu et al., 2020).

We use *fx*TWA-PLSv2 here. The evaluation is made by comparing the reconstructions made using modern pollen data with modern climates using leave-out cross-validation, where one site at a time is randomly selected as a test site and sites that are both geographically close (within 50 km horizontal distance from the site) and climatically close (within 2 % of the full range of each climate variable in the dataset) are also removed from the training set, to prevent redundancy in the climate information from inflating the cross-validation goodness of fit, following Liu et al. (2020). This ensures that we are not just tuning to the training dataset, and that we can reconstruct climates even when the training set does not completely cover the climate to be reconstructed because there are gaps in the climate space. Performance is assessed using R^2 and RMSEP (root-mean-square error of prediction), and compression is assessed using linear regression of the leave-out cross-validated reconstructions against the climate variable. The last significant number of components ($p \leq 0.01$) is selected to avoid overfitting due to the increase in the number of components. Reconstructions of MTCO, MTWA and α_{plant} are then made for every sample in each fossil record, using the last significant number of components. Sample-specific errors are estimated via bootstrapping (resampling the training set 1000 times) as described in Liu et al. (2020).

However, the low CO_2 at glacial period could lead to potential bias between reconstructed and actual plant-available moisture. Atmospheric CO_2 concentration has a direct impact on plant physiological processes, by modulating water-use efficiency (WUE), that is the ratio of carbon uptake to water loss through the stomata (Hatfield and Dold, 2019). The low CO_2 during the glacial period led to reduced water use efficiency (Farquhar, 1997; Gerhart and Ward, 2010; Prentice and Harrison, 2009). Strictly statistical reconstructions cannot take this into account since they are based on modern relationships between pollen assemblages and climate under recent CO_2 levels (Bartlein et al., 2011; Chevalier et al., 2020). Reconstructions based on inversion of a vegetation model (e.g. Garreta et al., 2010; Guiot et al., 2000; Izumi and Bartlein, 2016; Wu et al., 2007) implicitly account for the impact of CO_2 on vegetation composition, but the reconstructions are dependent on the reliability of the vegetation model and its sensitivity to CO_2 changes (Chevalier et al., 2020; Guiot et al., 2009). The actual conditions under low CO_2 should be wetter than the vegetation-based reconstructions of moisture variables (Prentice et al., 2017, 2022a). Prentice et al. (2022a) provide a correction method to account for variations on CO_2 based on combining eco-evolutionary optimality theory and experimental evidence on how the water-use efficiency as expressed by the ratio of leaf-internal to ambient CO_2 responds to variations in CO_2, as follows:

$$e(\text{MTGR}_1, \text{MI}_1, c_{\text{a}1}) = e(\text{MTGR}_0, \text{MI}_0, c_{\text{a}0}) \quad (1)$$

where e is the ratio of water loss to CO_2 uptake, a function of the mean temperature of the growing season (MTGR), moisture index (MI) and atmospheric CO_2 concentration (c_{a}). For MTGR and c_{a}, the subscript "1" denotes the past value, and the subscript "0" denotes the modern value. MI_0 is the reconstructed uncorrected past value, MI_1 is the "true" past value (to be estimated). The equation means that the "true" MI under past atmospheric conditions should produce the same e with the reconstructed uncorrected MI under modern atmospheric conditions, i.e. those pertaining to the modern pollen calibration dataset.

We transfer our reconstructed past α_{plant} back to the uncorrected moisture index MI_0, and apply the CO_2 correction to obtain the actual moisture index MI_1, then transfer it to actual plant-available moisture $\alpha_{\text{plant,corrected}}$ (Figs. 2 and S2a, b). Past and modern values of CO_2 concentrations are taken from Bereiter et al. (2015), following Prentice et al. (2022a). Past MTGR values are inferred by sinusoidal interpolation of reconstructed MTCO and MTWA, assuming that the growing season corresponds to the period with temperatures $> 0\,^{\circ}\text{C}$. Modern MTGR values are obtained using a geographically-weighted regression (GWR) of climatological values (1961–1990) from the Climatic Research Unit Time-Series version 4.04 (CRU TS4.04; Harris et al., 2020) dataset averaged over the period 1961–1990, in order to correct for elevation differences between the CRU grid cells and the fossil pollen sites.

Table 1. Site information of the fossil pollen records covering the interval 50–30 ka. The references with full citation are given in the Supplement, Sect. S3. lat is the latitude, lon is the longitude, elv is the elevation (unit: m). TERR means terrestrial record, MARI means marine record. n_{due} is the number of D–O events that should be found based on the time interval covered by the record. n_{miss} is the number of D–O events that were not identified. n_{low} is the number of D–O events missed because of low resolution of that part of the record. Some sites provide records in 50–30 ka but do not cover the intervals of the D–O events; some marine sites are too far from the land to extract GWR modern MTGR to apply CO_2 correction; these sites are all indicated by NA in n_{due}, n_{miss} and n_{low}.

name	lat	lon	elv	type	source	n_{due}	n_{miss}	n_{low}
Abric Romani	41.53	1.68	350	TERR	ACER	2	0	0
Akulinin Exposure P1282	47.12	138.55	20	TERR	Legacy2	1	0	0
Alut Lake	60.14	152.31	480	TERR	Cao et al. (2019, 2020)	7	1	1
Anderson Pond (ANDERSON)	36.03	−85.50	303	TERR	Legacy2	NA	NA	NA
Auel_AU2	50.28	6.59	457	TERR	AUTHOR	7	0	0
Aueler Maar_ELSA_AU3	50.28	6.60	456	TERR	Pangaea	3	0	0
Aueler Maar_ELSA_AU4	50.28	6.59	457	TERR	Pangaea	7	2	2
Azzano Decimo	45.88	12.72	10	TERR	ACER	4	0	0
Bajondillo	36.62	−4.50	20	TERR	Legacy2	2	0	0
Baldwin Lake	34.28	−116.81	2060	TERR	Legacy2	4	1	1
Balikun Lake	43.68	92.80	1575	TERR	Legacy2	NA	NA	NA
Balikun Lake BLK11A	43.68	92.80	1575	TERR	AUTHOR	2	0	0
Bambili 2	5.93	10.24	2323	TERR	Legacy2	5	1	1
Bandung DPDR-II	−6.99	107.73	662	TERR	Legacy2	4	2	2
Bay of Biscay	45.35	−5.22	−4100	MARI	Legacy2	NA	NA	NA
Bear Lake (BL00-1E)	41.95	−111.31	1805	TERR	ACER	7	2	2
Berelyekh River	63.28	147.75	800	TERR	Cao et al. (2019, 2020)	NA	NA	NA
Biggsville [Cessford Quarry]	40.86	−90.88	198	TERR	Legacy2	1	0	0
Bolotnyii Stream Exposure 117	42.85	132.78	4	TERR	Legacy2	2	1	1
Bolshoe Toko PG2133	56.04	130.87	903	TERR	Legacy2	2	0	0
Bolshoy Lyakhovsky Island	73.33	141.50	7	TERR	Legacy2	NA	NA	NA
Boney Spring	38.11	−93.37	210	TERR	Legacy2	1	1	1
Byllatskoye Exposure, Byllat River, Indigirka Basin	69.17	140.06	316	TERR	Legacy2	NA	NA	NA
Cala Conto	−17.57	−65.93	2700	TERR	Legacy2	2	2	2
Caledonia Fen	−37.33	146.73	1280	TERR	ACER	7	2	2
Cambara do Sul	−29.05	−50.10	1040	TERR	ACER	7	2	0
Camel Lake	30.26	−85.01	20	TERR	ACER	2	1	1
Carp Lake	45.91	−120.88	720	TERR	ACER	8	3	3
Changping CHZK1	40.18	116.22	49	TERR	Zhou et al. (2023)	NA	NA	NA
Chenghai CH2	23.48	116.80	5	TERR	Zhou et al. (2023)	4	1	1
Cheremushka Bog	52.75	108.08	1500	TERR	Cao et al. (2019, 2020)	1	0	0
Colonia	−23.87	−46.71	900	TERR	ACER	7	5	5
Colonia CO3	−23.87	−46.71	900	TERR	Legacy2	7	4	4
Core Trident 163 31B	−3.61	−83.96	−3210	MARI	ACER	NA	NA	NA
Correo	44.56	6.00	1100	TERR	Legacy2	1	0	0
Crystal Lagoon	−40.48	148.35	8	TERR	Legacy2	1	0	0
Daihai Lake-Wajianggou	40.58	112.67	1500	TERR	Zhou et al. (2023)	NA	NA	NA
Dajiu Lake DJH-1	31.49	110.00	1751	TERR	Zhou et al. (2023)	8	1	1
Dalai Nur Lake-Haiyan	43.28	116.58	1200	TERR	Zhou et al. (2023)	NA	NA	NA
Daluoba	47.83	88.20	2020	TERR	Zhou et al. (2023)	NA	NA	NA
Dar Fatma	36.82	8.77	780	TERR	Legacy2	7	2	2
Daxing DZK1	39.72	116.32	49	TERR	Zhou et al. (2023)	NA	NA	NA
Dead Sea	31.51	35.47	−428	TERR	Pangaea	6	0	0
Demyanskoye	59.50	69.50	65	TERR	Cao et al. (2019, 2020)	1	0	0
Deva-Deva	−7.12	37.62	2600	TERR	Legacy2	4	1	1
Diexi Lake	32.04	103.68	2334	TERR	Zhou et al. (2023)	2	0	0
Dikikh Olyenyeii Lake	67.75	−178.83	300	TERR	Cao et al. (2019, 2020)	3	1	1
Eastern Niger Delta	4.55	6.43	0	TERR	Legacy2	NA	NA	NA
Elikchan 4 Lake	60.75	151.88	810	TERR	Cao et al. (2019, 2020)	3	1	1
Emanda	65.29	135.76	671	TERR	Legacy2	4	1	1
Enmynveem River (mammoth site)	68.17	165.93	400	TERR	Legacy2	NA	NA	NA
Enmynveem River1	68.17	165.93	400	TERR	Cao et al. (2019, 2020)	NA	NA	NA
Erlongwan Maar Lake	42.30	126.37	724	TERR	Zhou et al. (2023)	2	0	0
Ershilipu	36.93	116.65	50	TERR	Zhou et al. (2023)	NA	NA	NA

Table 1. Continued.

name	lat	lon	elv	type	source	n_{due}	n_{miss}	n_{low}
EW9504-17 PC	42.23	−125.81	−2671	MARI	ACER	NA	NA	NA
F2-92-P29	32.90	−119.73	−1475	MARI	ACER	2	2	2
Faddeyevskiy	75.33	143.83	30	TERR	Legacy2	NA	NA	NA
Fargher Lake	45.88	−122.58	200	TERR	ACER	8	2	1
Feng Suancigou Feng	35.51	105.81	1840	TERR	Zhou et al. (2023)	1	1	1
Fog Lake	67.18	−63.25	422	TERR	Legacy2	2	1	1
Fundo Nueva	−41.28	−73.83	66	TERR	ACER	5	1	0
Fuquene	5.45	−73.46	2540	TERR	ACER	7	3	3
Furamoos	47.98	9.88	662	TERR	ACER	NA	NA	NA
Gantang SZY	26.77	119.03	1007	TERR	Zhou et al. (2023)	5	1	1
GeoB2107-3	−27.18	−46.45	−1048	MARI	Legacy2	NA	NA	NA
GeoB3104	−3.67	−37.72	−767	MARI	ACER	1	1	1
Girraween Lagoon	−12.52	131.08	25	TERR	AUTHOR	5	1	1
Goshen Springs	31.72	−86.13	105	TERR	Legacy2	2	2	2
Grass Lake	41.65	−122.17	1537	TERR	Legacy2	3	0	0
Grays Lake (GRAYSGL1)	43.07	−111.44	1195	TERR	Legacy2	4	1	1
Grays Lake (GRAYSGL6)	43.07	−111.44	1195	TERR	Legacy2	NA	NA	NA
Guangzhou GZ-2	22.71	113.51	1	TERR	Zhou et al. (2023)	3	2	2
Guangzhou GZ-4	23.27	113.21	4	TERR	Zhou et al. (2023)	1	0	0
Gytgykai Lake	63.42	176.57	102	TERR	Cao et al. (2019, 2020)	1	0	0
Hachihama	34.55	133.95	6	TERR	Legacy2	3	1	1
Hangzhou HQB7	30.47	120.21	2	TERR	Zhou et al. (2023)	1	0	0
Hay Lake	34.00	−109.43	2780	TERR	ACER	NA	NA	NA
Headwaters Opasnaya River	48.23	138.48	1320	TERR	Legacy2	NA	NA	NA
Hosoike Moor	35.35	134.13	970	TERR	Legacy2	4	2	2
Huguangyan Maar Lake B	21.15	110.28	88	TERR	Zhou et al. (2023)	NA	NA	NA
Huinamarca (Lake Titicaca)	−16.23	−68.77	3810	TERR	ACER	3	0	0
Indigirka lowlands	70.58	145.00	20	TERR	Cao et al. (2019, 2020)	1	0	0
Ioannina	39.75	20.85	470	TERR	ACER	8	1	0
IODP Site 353-U1446A	19.08	85.73	−1430.2	MARI	Pangaea	6	1	1
Iwaya site	35.52	135.89	20	TERR	Legacy2	3	1	1
Jackson Pond (JACKSN07)	37.43	−85.72	260	TERR	Legacy2	NA	NA	NA
Jiangcun	34.40	109.50	650	TERR	Zhou et al. (2023)	3	0	0
Joe Lake	66.77	−157.22	183	TERR	ACER	3	1	1
Julietta Lake	61.34	154.56	880	TERR	Cao et al. (2019, 2020)	3	0	0
Kai Iwa	−35.82	173.65	70	TERR	AUTHOR	6	2	2
Kaiyak Lake	68.14	−161.44	190	TERR	Legacy2	NA	NA	NA
Kalaloch	47.63	−124.38	24	TERR	Legacy2	8	1	0
Kalistratikha	53.33	83.25	190	TERR	Cao et al. (2019, 2020)	NA	NA	NA
Kalistratikha Exposure	53.33	83.25	190	TERR	Legacy2	NA	NA	NA
Kamiyoshi Basin (KY01)	35.10	135.59	335	TERR	ACER	1	0	0
Kashiru Bog	−3.47	29.57	2240	TERR	ACER	NA	NA	NA
Kenbuchi Basin	44.05	142.38	135	TERR	ACER	3	0	0
Khoe	51.34	142.14	15	TERR	ACER	1	0	0
Khoe, Sakhalin Island	51.34	142.14	15	TERR	Cao et al. (2019, 2020)	4	2	2
Kirgirlakh Stream, Berelyekh River Basin (DIMA2)	62.67	147.98	700	TERR	Legacy2	NA	NA	NA
Kirgirlakh Stream, Berelyekh River Basin (DIMA3)	62.67	147.98	700	TERR	Legacy2	1	0	0
Kirgirlakh Stream_2	62.67	147.98	700	TERR	Cao et al. (2019, 2020)	1	1	1
Kohuora	−36.95	174.87	5	TERR	ACER	NA	NA	NA
Komanimambuno Mire	−5.82	145.09	2740	TERR	Legacy2	NA	NA	NA
Kunming Basin KZ2-3	25.00	102.62	1890	TERR	Zhou et al. (2023)	NA	NA	NA
Kupena (KUPENA3)	41.98	24.33	1356	TERR	Legacy2	NA	NA	NA
Kurota Lowland	35.52	135.88	20	TERR	ACER	1	0	0
KW31	3.52	5.57	−1181	MARI	ACER	1	0	0
La Laguna	4.92	−74.03	2900	TERR	ACER	1	0	0
Labaz lake (LAO6-95)	72.29	99.61	42	TERR	Legacy2	2	1	0
Lac du Bouchet – DIGI	44.83	3.82	1200	TERR	ACER	8	1	0
Lac Emeric	−22.30	166.97	230	TERR	Legacy2	3	1	1
Lac Suprin	−22.29	166.99	235	TERR	Legacy2	4	2	2
Lagaccione	42.57	11.80	355	TERR	ACER	3	0	0

Table 1. Continued.

name	lat	lon	elv	type	source	n_{due}	n_{miss}	n_{low}
Lago Grande di Monticchio	40.94	15.61	656	TERR	ACER	8	0	0
Lagoa Campestre de Salitre (SALILC3)	−19.00	−46.77	980	TERR	Legacy2	3	2	2
Lagoa das Patas	0.27	−66.68	300	TERR	Legacy2	4	1	1
Laguna Bella Vista	−13.62	−61.55	600	TERR	ACER	2	1	1
Laguna Chaplin	−14.47	−61.07	600	TERR	ACER	NA	NA	NA
Laguna Ciega	6.48	−72.39	3510	TERR	Legacy2	NA	NA	NA
Laguna Junin	−11.00	−76.17	4100	TERR	Legacy2	5	2	2
Lake Ailike	46.54	86.36	278	TERR	AUTHOR	5	0	0
Lake Albert (Lake Mobutu Sese Seko)	1.83	31.17	619	TERR	Legacy2	NA	NA	NA
Lake Annie	27.21	−81.35	34	TERR	Legacy2	1	0	0
Lake Baikal_BDP99	52.09	105.84	456	TERR	Pangaea	7	0	0
Lake Billyakh	65.28	126.78	340	TERR	ACER	3	0	0
Lake Biwa (BIW95-4)	35.25	136.05	84	TERR	ACER	3	0	0
Lake Carpentaria	−12.52	140.35	−60	MARI	Legacy2	4	2	2
Lake Chalco CHA08	19.25	−98.97	2250	TERR	AUTHOR	5	1	1
Lake Consuelo (CON1)	−13.95	−68.99	1360	TERR	ACER	7	2	2
Lake E5	68.64	−149.46	803	TERR	Legacy2	NA	NA	NA
Lake Elsinore	33.66	−117.35	376	TERR	Legacy2	1	0	0
Lake Fimon	45.47	11.53	23	TERR	AUTHOR	NA	NA	NA
Lake George	−35.09	149.43	673	TERR	Legacy2	4	0	0
Lake Hordorli	−2.54	140.59	798	TERR	Legacy2	4	0	0
Lake Iznik	40.43	29.53	88	TERR	Legacy2	1	0	0
Lake Malawi	−11.22	34.42	470	TERR	ACER	5	2	2
Lake Masoko	−9.33	33.75	840	TERR	ACER	2	1	1
Lake Nero (NERO2)	57.18	39.45	93	TERR	Legacy2	NA	NA	NA
Lake Nojiri	36.83	138.22	657	TERR	ACER	8	0	0
Lake Patzcuaro	19.58	−101.58	2044	TERR	Legacy2	2	1	1
Lake Peten-Itza	16.99	−89.82	110	TERR	Legacy2	8	1	1
Lake Quexil	16.92	−89.82	110	TERR	Legacy2	4	2	2
Lake Selina	−41.88	145.61	516	TERR	Legacy2	1	0	0
Lake Tanganyika (KH3)	−8.50	30.75	773	TERR	Legacy2	4	2	2
Lake Tanganyika (KH4)	−8.50	30.75	773	TERR	Legacy2	NA	NA	NA
Lake Tanganyika [north basin] (SD24TAN)	−4.19	29.31	773	TERR	Legacy2	NA	NA	NA
Lake Tritrivakely	−19.78	46.92	1778	TERR	Legacy2	5	1	0
Lake Tulane	29.83	−81.95	36	TERR	ACER	7	1	1
Lake Wangoom LW87 core	−38.35	142.60	100	TERR	ACER	4	0	0
Lake Xinias	39.05	22.27	500	TERR	ACER	8	3	3
Lake Yamozero	65.02	50.23	213	TERR	Legacy2	2	0	0
Lake Zeribar	35.53	46.12	1288	TERR	Legacy2	7	1	1
Ledovyi Obryv Exposure, Northern Section	64.10	171.18	57	TERR	Legacy2	NA	NA	NA
Les Echets G – DIGI	45.90	4.93	267	TERR	ACER	8	0	0
Levantine Basin	32.03	34.28	0	TERR	Legacy2	4	1	1
Levinson Lessing Lake PG1228	74.47	98.64	47	TERR	Cao et al. (2019, 2020)	1	0	0
Little Lake	44.16	−123.58	217	TERR	ACER	5	0	0
Lop Nur K1	40.28	90.25	780	TERR	Zhou et al. (2023)	NA	NA	NA
Luanhaizi Lake LH2	37.59	101.35	3200	TERR	Zhou et al. (2023)	1	0	0
Luochuan	35.75	109.42	1068	TERR	Zhou et al. (2023)	NA	NA	NA
Lynchs Crater	−17.37	145.70	760	TERR	ACER	7	4	4
Malyi Krechet Lake	64.80	175.53	32	TERR	Legacy2	2	0	0
Mamontovy Khayata	71.77	129.45	0	TERR	Cao et al. (2019, 2020)	3	0	0
Mamontovy Klyk	73.61	117.13	25	TERR	Legacy2	1	0	0
MD01-2421	36.02	141.77	−2224	MARI	ACER	8	1	0
MD03-2622 Cariaco Basin	10.71	−65.17	−877	MARI	ACER	7	5	3
MD04-2845	45.35	−5.22	−4100	MARI	ACER	NA	NA	NA
MD84-629	32.07	34.35	−745	MARI	ACER	5	1	1
MD95-2039	40.58	−10.35	−3381	MARI	ACER	8	1	1
MD95-2042	37.80	−10.17	−3148	MARI	ACER	8	1	1
MD95-2043	36.14	−2.62	−1841	MARI	ACER	8	1	1
MD99-2331	41.15	−9.68	−2110	MARI	ACER	7	1	1
Megali Limni	39.10	26.32	323	TERR	ACER	6	0	0

Table 1. Continued.

name	lat	lon	elv	type	source	n_{due}	n_{miss}	n_{low}
Melkoye Lake	64.86	175.23	36	TERR	Cao et al. (2019, 2020)	1	0	0
Mereya River	46.62	142.92	4	TERR	Cao et al. (2019, 2020)	NA	NA	NA
Mfabeni Peatland	−28.15	32.52	11	TERR	ACER	4	1	0
Middle Butte Cave	43.37	−112.62	1590	TERR	Legacy2	NA	NA	NA
Milin	29.31	94.35	2982	TERR	Zhou et al. (2023)	3	0	0
Moershoofd	51.25	3.52	2	TERR	Legacy2	NA	NA	NA
Morro de Itapeva	−22.78	−45.53	1850	TERR	Legacy2	NA	NA	NA
Mud Lake (MUDLAKE)	29.30	−81.87	9	TERR	Legacy2	4	1	1
Muscotah Marsh	39.53	−95.51	280	TERR	Legacy2	NA	NA	NA
Nachtigall	51.81	9.40	95	TERR	Legacy2	NA	NA	NA
Nakafurano	43.37	142.43	173	TERR	ACER	2	1	1
Native Companion Lagoon	−27.68	153.41	20	TERR	ACER	4	2	2
Navarres	39.10	−0.68	225	TERR	ACER	3	0	0
Ngamakala Pound (GAMA4)	−4.08	15.38	400	TERR	Legacy2	NA	NA	NA
Ngoring Lake CK6	34.92	97.73	4272	TERR	Zhou et al. (2023)	NA	NA	NA
Noordzee T121	54.10	4.21	0	TERR	Legacy2	NA	NA	NA
Northern Coast of Onemen Gulf	64.78	176.17	18	TERR	Legacy2	3	0	0
ODP 1233 C	−41.00	−74.45	−838	MARI	ACER	8	2	1
ODP 1234	−36.22	−73.68	−1015	MARI	ACER	8	0	0
ODP 820	−16.63	146.30	−280	MARI	ACER	5	3	3
ODP site 976	36.20	−4.30	−1108	MARI	ACER	8	1	0
ODP1019	41.66	−124.91	989	MARI	ACER	7	3	3
ODP1078C	−11.92	13.40	−426	MARI	ACER	8	2	1
ODP893A	34.28	−120.03	−577	MARI	ACER	8	0	0
Oil Lake	70.29	−151.17	745	TERR	Legacy2	2	0	0
Okarito Pakihi	−43.24	170.22	70	TERR	ACER	NA	NA	NA
Ovrazhnyi Stream-2	43.25	134.57	10	TERR	Cao et al. (2019, 2020)	NA	NA	NA
Ovrazhnyii-1 Stream Exposure	43.25	134.57	8	TERR	Legacy2	NA	NA	NA
Ovrazhnyii-2 Exposure 667-842	43.25	134.57	10	TERR	Legacy2	NA	NA	NA
Padul	37.01	−3.60	726	TERR	AUTHOR	6	2	2
Paramonovskii Stream	43.20	133.75	120	TERR	Cao et al. (2019, 2020)	NA	NA	NA
Paramonovskii Stream Exposure 4980	43.20	133.75	120	TERR	Legacy2	NA	NA	NA
Pavlovka Exposure 988	44.32	134.00	300	TERR	Legacy2	NA	NA	NA
Peloncillo Mountains	32.29	−109.09	1400	TERR	Legacy2	NA	NA	NA
Peschanka Exposure 155	43.30	132.12	12	TERR	Legacy2	NA	NA	NA
Pittsburg Basin	38.90	−89.19	162	TERR	Legacy2	NA	NA	NA
Plesheevo Lake	56.77	38.78	148	TERR	Legacy2	2	0	0
Potato Lake	34.45	−111.33	2222	TERR	ACER	1	1	1
Poutu	−36.38	174.13	82	TERR	AUTHOR	1	1	1
Pretoria Saltpan	−25.41	28.08	1150	TERR	Legacy2	4	0	0
Qingdao ZK2	36.29	120.46	31	TERR	Zhou et al. (2023)	NA	NA	NA
Qingdao ZK3	36.26	120.64	7	TERR	Zhou et al. (2023)	NA	NA	NA
Rahue	−39.37	−70.93	1000	TERR	Legacy2	NA	NA	NA
Reenadinna Wood	52.01	−9.53	20	TERR	Legacy2	NA	NA	NA
Rice Lake (Rice Lake 81)	40.30	−123.22	1100	TERR	ACER	NA	NA	NA
Rietvlei-Still Bay	−34.35	21.54	17	TERR	Legacy2	NA	NA	NA
Rio Timbio	2.37	−76.71	1750	TERR	Legacy2	NA	NA	NA
Rockyhock Bay	36.17	−76.68	6	TERR	Legacy2	NA	NA	NA
Ruby Marsh	41.13	−115.51	1818	TERR	Legacy2	1	0	0
Rusaka Swamp	−3.43	29.62	2070	TERR	Legacy2	1	0	0
Sacred Lake	0.05	37.53	2345	TERR	Legacy2	3	2	2
Saint-Ursin	48.52	−0.25	234	TERR	Legacy2	3	0	0
San Agustin Plains (SAPBHM)	33.87	−108.25	2069	TERR	Legacy2	NA	NA	NA
Sangluoshu	37.50	117.73	50	TERR	Zhou et al. (2023)	NA	NA	NA
Sanshui K5	22.78	112.63	12	TERR	Zhou et al. (2023)	NA	NA	NA
Shaamar	50.20	105.20	650	TERR	Legacy2	2	0	0
Shuidonggou SDG2	38.28	106.50	1200	TERR	Zhou et al. (2023)	NA	NA	NA
Shunyi GZK1	40.15	116.53	50	TERR	Zhou et al. (2023)	NA	NA	NA
Siberia	−17.09	−64.72	2920	TERR	ACER	1	1	1

Table 1. Continued.

name	lat	lon	elv	type	source	n_{due}	n_{miss}	n_{low}
Siberia1	−17.09	−64.72	2920	TERR	Legacy2	1	1	1
Sihailongwan Maar Lake	42.28	126.60	797	TERR	Pangaea	8	1	1
Siluyanov Yar-2 Exposure	46.13	137.83	25	TERR	Legacy2	NA	NA	NA
Sirunki Wabag	−5.44	143.53	2550	TERR	Legacy2	2	0	0
St. Catherines Island (Northwest Marsh)	31.69	−81.15	0	TERR	Legacy2	NA	NA	NA
Stoneman Lake_STL	34.78	−111.52	2048	TERR	AUTHOR	3	0	0
Stracciacappa	42.13	12.32	220	TERR	ACER	4	0	0
Straldzha mire (QUARRY)	42.63	26.78	137	TERR	Legacy2	NA	NA	NA
Tagua Tagua – DIGI	−34.50	−71.16	200	TERR	ACER	6	1	1
Taiquemo	−42.17	−73.60	170	TERR	ACER	8	0	0
Tanon River	59.67	151.20	40	TERR	Cao et al. (2019, 2020)	NA	NA	NA
Tanon River [Quarry Site]	59.67	151.20	40	TERR	Legacy2	NA	NA	NA
Taymyr Lake SAO1	74.55	100.53	47	TERR	Cao et al. (2019, 2020)	NA	NA	NA
Tianshuihai TS95	35.35	79.52	4900	TERR	Zhou et al. (2023)	1	0	0
Tianyang Maar Lake TYC	20.52	110.30	108	TERR	Zhou et al. (2023)	3	0	0
Tianyang TY1	20.35	110.35	90	TERR	Zhou et al. (2023)	1	1	0
Tikhangou Exposure	42.83	132.78	4	TERR	Legacy2	NA	NA	NA
Toadlena Lake [Dead Man Lake] (DEAD5826)	36.24	−108.95	2759	TERR	Legacy2	1	0	0
Toadlena Lake [Dead Man Lake] (DEAD6101)	36.24	−108.95	2759	TERR	Legacy2	4	2	2
Tortoise Lagoon	−27.52	153.47	39	TERR	Legacy2	2	2	2
Toushe Basin	23.82	120.88	650	TERR	ACER	8	0	0
Toushe Lake 2013	23.82	120.88	650	TERR	Zhou et al. (2023)	1	0	0
Tswaing Crater	−25.40	28.08	1100	TERR	ACER	5	0	0
Tukuto Lake	68.50	−157.03	505	TERR	Legacy2	1	1	1
Tyrrendara Swamp	−38.20	141.76	13	TERR	ACER	NA	NA	NA
Ulan Buh Desert WL10ZK-1	40.04	105.78	1026	TERR	Zhou et al. (2023)	NA	NA	NA
Valle di Castiglione	41.90	12.76	44	TERR	ACER	7	3	3
Villarquemado	40.82	−1.48	985	TERR	AUTHOR	4	1	0
Vinillos	−0.60	−77.85	2090	TERR	Legacy2	1	0	0
Voordrag	−27.74	31.33	940	TERR	Legacy2	NA	NA	NA
W8709-13 PC	42.11	−125.75	−2712	MARI	ACER	NA	NA	NA
W8709-8 PC	42.26	−127.68	−3111	MARI	ACER	NA	NA	NA
Walker Lake	35.38	−111.71	2500	TERR	ACER	NA	NA	NA
Wenquangou	35.92	94.20	4700	TERR	Zhou et al. (2023)	NA	NA	NA
White Pond (WHITESC)	34.17	−80.78	90	TERR	Legacy2	NA	NA	NA
Wulagai Lake	45.42	117.48	822	TERR	AUTHOR	7	0	0
Xere Wapo	−22.30	166.96	235	TERR	Legacy2	NA	NA	NA
Xijir Ulan Lake	35.23	90.33	4500	TERR	Zhou et al. (2023)	NA	NA	NA
Xining ZK2	35.97	101.67	4363	TERR	Zhou et al. (2023)	NA	NA	NA
Yabulai Mt	39.62	103.92	1266	TERR	Zhou et al. (2023)	2	0	0
Yangerzhuang	38.35	117.35	5	TERR	Zhou et al. (2023)	NA	NA	NA
Yangjiapo	40.02	118.68	70	TERR	Zhou et al. (2023)	NA	NA	NA
Yangyuan-Caocun	40.10	114.40	875	TERR	Zhou et al. (2023)	1	0	0
Yaxi Co Lake	34.28	92.67	4000	TERR	Zhou et al. (2023)	NA	NA	NA
Zagoskin Lake	63.45	−162.11	7	TERR	Legacy2	5	0	0
Zhongshan PK19	21.80	113.30	6	TERR	Zhou et al. (2023)	NA	NA	NA

The elevations of marine sites are set to 0 when applying GWR.

The CO_2 correction is implemented through the package COdos 0.0.2 (Prentice et al., 2022b) with one modification, as follows. We found when applying the correction in cases where the temperature reduction from modern was large ($> 5\,°C$) that the use of different temperature values to calculate the stomatal sensitivity term (ξ) and the compensation point (Γ^*) in the correction algorithm sometimes produced an unrealistically large countervailing effect due to the temperature difference alone. To avoid this problem, we calculate these physiological quantities (ξ and Γ^*) using the mean of $MTGR_1$ and $MTGR_0$.

2.3 Age modelling of fossil records

Both the ACER and ACER2 database provide age models for each pollen record. However, the resolution of the individual records are variable (ranging from 57 years to 13 415 years) and these age models are often imperfectly aligned with the dating of D–O warming events as recorded in the

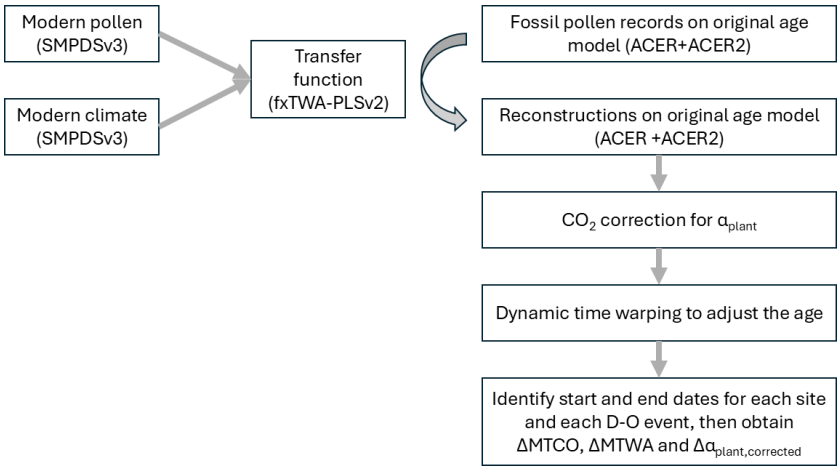

Figure 2. Flow chart showing the methodology.

Greenland ice core, and which have been shown to have a globally synchronous imprint through analysis of speleothem records (Adolphi et al., 2018; Corrick et al., 2020). To create a better alignment, we use dynamic time warping (DTW: Alshehri et al., 2019; Burstyn et al., 2021; Giorgino, 2009) to adjust the age scale for each individual record (Fig. 2). Dynamic time warping optimises the similarity between two sequences (one "query" and one "reference") by stretching or compressing one sequence in the time dimension to match the other. It adjusts the age scale without influencing the variable values, thus retaining the original amplitude of change.

The LOVECLIM simulation (Menviel et al., 2014) (covering the interval 50–30 ka) is currently the only published simulation that has attempted to reproduce the specific timing and magnitude of successive D–O cycles. It is a coupled ocean-atmosphere-vegetation general circulation model of intermediate complexity. The model was spun up to equilibrium using an initial atmospheric CO_2 concentration of 207.5 ppm, orbital forcing appropriate for 50 ka BP, and an estimate of the 50 ka BP ice-sheet orography and albedo obtained from an off-line ice-sheet model simulation (Abe-Ouchi et al., 2007). After this initialization, the model was forced by time-varying changes in orbital parameters, atmospheric trace gas concentrations and ice-sheet configurations following Timm et al. (2008). In addition, meltwater pulses were added in the North Atlantic in such a way as to reproduce observed sea-surface temperature (SST) variations along the Iberian margin (Martrat et al., 2007). The simulations have proved adequate to capture at least the broad features of actual D–O events, and are generally consistent with the qualitative signals in Voelker (2002) compilation (Liu et al., 2022). We convert the age scale of LOVECLIM simulations to match the Antarctic Ice Core Chronology 2012 (AICC2012) time scale (Veres et al., 2013).

We treat the mean annual temperature (MAT) calculated as the average of MTCO and MTWA reconstructed from each individual fossil pollen record as the "query" time series, and find the corresponding grid cell (the location of the fossil pollen record) in the LOVECLIM simulations, and use the simulated MAT at this grid cell as the "reference" time series. We further divide each "query" and "reference" time series into discrete intervals using the mid-points between the start dates of each D–O warming event as recorded in the Greenland ice core (Wolff et al., 2010; converted into AICC2012 timescale), and normalize both time series in each interval to remove the influence of differences in absolute values and the amplitude of changes. Then we apply dynamic time warping to modify the time scale of the "query" to match the "reference" in each interval. The adjusted age model for each fossil record is then applied to the reconstructions of MTCO, MTWA, α_{plant} and $\alpha_{plant,corrected}$ from that record for subsequent analyses.

2.4 Assessment of regional climate changes during Greenland D–O warming events

The magnitude of climate change during the interval corresponding to each D–O warming event as registered in Greenland is calculated individually for each climate variable at each site. To avoid making an assumption about the sign of the climate change at a site, we use a third-order polynomial to fit the reconstructions during the interval from 300 years before to 600 years after the official start date corresponding to Greenland D–O warming for each event (Wolff et al., 2010; converted into AICC2012 timescale) to determine whether the change was positive or negative. We then find the ages where this polynomial curve reaches the minimum and maximum ($t_{min,polynomial}$ and $t_{max,polynomial}$). Since the smoothed polynomial may underestimate or overestimate the amplitude of change, we use the reconstructions corresponding to $t_{min,polynomial}$ and $t_{max,polynomial}$ to obtain the changes (see Fig. S3 for illustration). Whether it's an increasing or decreasing signal depends on whether $t_{min,polynomial}$ occurs be-

fore or after $t_{\max,\text{polynomial}}$. The change of each climate variable (ΔV) is calculated as:

$$\Delta V = V_{\text{end}} - V_{\text{start}} \quad (2)$$

where V_{start} is the reconstructed value at the start and V_{end} is the reconstructed value at the end of the event. The error of change ($\sigma_{\Delta V}$) is calculated using the following equation assuming V_{start} and V_{end} are independent:

$$\sigma_{\Delta V} = \sqrt{\sigma^2_{V_{\text{end}}} + \sigma^2_{V_{\text{start}}}} \quad (3)$$

where $\sigma_{V_{\text{start}}}$ is the sample-specific error of V_{start} and $\sigma_{V_{\text{end}}}$ is the sample-specific error of V_{end}.

To obtain the relationships between changes in different climate variables, we use a maximum likelihood method to estimate the ratio of ΔMTCO to ΔMTWA and the ratio of $\Delta\alpha_{\text{plant,corrected}}$ to ΔMTWA to take account of the errors on both variables, following Liu et al. (2022).

As a measure of the accuracy of the DTW method to identify D–O events, we compare the number of identified events with the number of D–O events that should occur during the time covered by each record (Table 1). To assess whether events are missed in a particular record due to low sampling resolution, we examine the number of samples present in the 900-year interval covering the sampled D–O (i.e. 300 years before to 600 years after the official start date corresponding to Greenland D–O warming for each event), where low resolution is defined as ≤ 3 samples in this 900-year interval.

3 Results

*fx*TWA-PLS reproduces the modern climate reasonably well (Table 2; Fig. S4a, b). The performance is best for MTCO ($R^2 = 0.74$, RMSEP = 6.66, slope = 0.84) but is also good for MTWA ($R^2 = 0.60$, RMSEP = 3.63, slope = 0.72) and α_{plant} ($R^2 = 0.63$, RMSEP = 0.186, slope = 0.68). Assessment of the variance inflation factor scores shows that there is no problem of multicollinearity so that it is possible to reconstruct all three climate variables independently (Table S1).

The use of dynamic time warping makes it possible to identify D–O events robustly (Fig. S5a–h; Tables 1 and S2). Some sites provide records in 50–30 ka but do not cover the intervals of the D–O events; some marine sites are too far from the land to extract GWR modern MTGR to apply the CO_2 correction. Across the remaining 179 sites which should have D–O events registered, we have identified 544 out of the 696 individual events (78 %). In the majority of cases where a D–O event should have been registered but could not be identified in an individual record (134 out of 152 cases), the resolution of that part of the record is extremely poor.

ΔMTCO is found to be significantly larger than ΔMTWA in the northern extratropics and tropics when considered across all D–O events and sites, indicating reduced seasonal contrast between winter and summer temperatures; ΔMTCO is found to be larger than ΔMTWA, but not significantly larger, in the southern extratropics (Fig. 3; Table 3). There is no globally consistent relationship between $\Delta\alpha_{\text{plant,corrected}}$ and ΔMTWA, although the positive relationship in the tropics is marginally significant (Fig. 4; Table 4).

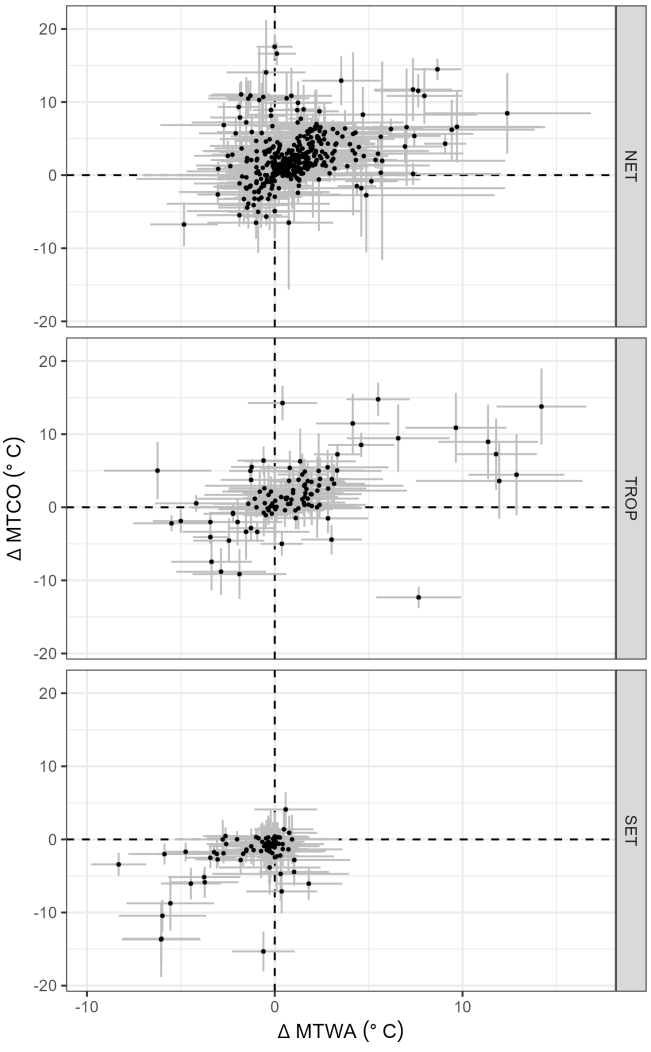

Figure 3. Scatter plot of the change in mean temperature of the coldest month (ΔMTCO) versus the change in mean temperature of the warmest month (ΔMTWA) during individual Dansgaard–Oeschger (D–O) events at individual sites. The points are grouped into the northern extratropics (NET, north of 23.5° N), the tropics (TROP, between 23.5° N and 23.5° S) and the southern extratropics (SET, south of 23.5° S). The grey lines indicate ±1 error of the change.

The spatial patterns of ΔMTCO and ΔMTWA are generally consistent across multiple D–O events (Fig. 5), most noticeably that the largest warming occurs in Eurasia, while western North America and the southern extratropics are characterised by cooling. These patterns are also shown if only reconstructions where the change is twice the error of change are considered (Fig. S6), proving that the spatial pat-

Table 2. Leave-out cross-validation (with geographically and climatically close sites removed) using fxTWA-PLSv2, for mean temperature of the coldest month (MTCO), mean temperature of the warmest month (MTWA) and plant-available moisture (α_{plant}). P-splines smoothed *fx* was estimated using 200 bins. n is the number of components used; Avg.bias is the average bias; RMSEP is the root-mean-square error of prediction; ΔRMSEP% is the per cent change of RMSEP of the current number of components compared to using one component less, i.e. $100 \times (\mathrm{RMSEP}_n - \mathrm{RMSEP}_{n-1}) / \mathrm{RMSEP}_{n-1}$. The p value assesses whether using the current number of components represents a significant ($p \leq 0.01$) difference over using one fewer component. To avoid over-fitting, the last significant number of components (i.e. the first insignificant number of components minus 1; p can become significant again after being insignificant with increasing n, but this is regarded meaningless) is selected for subsequent analyses and indicated in bold. The degree of overall compression is assessed by linear regression of the cross-validated reconstructions against the variable; b_1 and σ_{b_1} are the slope and the standard error of the slope, respectively. A slope (b_1) of 1 indicates no compression. NA means that no value could be calculated for ΔRMSEP% and p when $n = 1$, since they are defined based on comparison with using one fewer component.

	n	R^2	Avg.bias	RMSEP	ΔRMSEP%	p	b_1	σ_{b_1}
MTCO (°C)	1	0.72	−1.15	6.89	NA	NA	0.82	0.00
	2	0.73	−1.25	6.75	−2.00	0.001	0.83	0.00
	3	**0.74**	**−1.20**	**6.66**	**−1.42**	**0.001**	**0.84**	**0.00**
	4	0.74	−1.23	6.66	0.02	0.663	0.84	0.00
	5	0.74	−1.24	6.64	−0.31	0.001	0.84	0.00
	6	0.74	−1.24	6.63	−0.11	0.001	0.84	0.00
MTWA (°C)	1	0.51	−0.32	4.00	NA	NA	0.64	0.00
	2	0.59	−0.22	3.67	−8.32	0.001	0.72	0.00
	3	**0.60**	**−0.25**	**3.63**	**−0.95**	**0.001**	**0.72**	**0.00**
	4	0.60	−0.25	3.62	−0.29	0.012	0.72	0.00
	5	0.60	−0.27	3.63	0.22	0.974	0.72	0.00
	6	0.60	−0.28	3.61	−0.61	0.001	0.72	0.00
α_{plant}	1	0.61	−0.020	0.191	NA	NA	0.65	0.00
	2	0.62	−0.022	0.190	−0.49	0.001	0.67	0.00
	3	**0.63**	**−0.020**	**0.186**	**−2.07**	**0.001**	**0.68**	**0.00**
	4	0.64	−0.020	0.186	−0.30	0.020	0.69	0.00
	5	0.64	−0.020	0.185	−0.18	0.003	0.70	0.00
	6	0.64	−0.020	0.185	0.09	0.988	0.70	0.00

Table 3. Maximum likelihood estimates of the relationship between the change in mean temperature of the coldest month (ΔMTCO) and the change in mean temperature of the warmest month (ΔMTWA) for the northern extratropics (NET, north of 23.5° N), tropics (TROP, between 23.5° N and 23.5° S) and southern extratropics (SET, south of 23.5° S). The intercepts were set to zero since both variables are changes.

Region		Coefficient	Standard error (SE)	Lower 95 %	Upper 95 %
NET	Slope	2.9	0.5	2.0	3.8
TROP	Slope	2.1	0.4	1.2	3.0
SET	Slope	1.5	0.7	0.2	2.8

Table 4. Maximum likelihood estimates of the relationship between the change in CO_2-corrected plant-available moisture ($\Delta\alpha_{plant,corrected}$) and the change in mean temperature of the warmest month (ΔMTWA) for the northern extratropics (NET, north of 23.5° N), tropics (TROP, between 23.5° N and 23.5° S) and southern extratropics (SET, south of 23.5° S). The intercepts were set to zero since both variables are changes.

Region		Coefficient	Standard error (SE)	Lower 95 %	Upper 95 %
NET	Slope	0.27	0.24	−0.21	0.74
TROP	Slope	0.02	0.01	0.01	0.04
SET	Slope	−0.03	0.02	−0.06	0.01

terns are robust to the choice of threshold. Nevertheless, both the magnitude of the changes and the spatial patterns vary between the D–O events (Fig. S7a, b). Strong events such as D–O 8 show more apparent changes (whether warming or cooling), as well as a strong antiphasing between northern and southern extratropical changes; while weak events such as D–O 9 show less apparent changes with almost no north-south antiphasing (Fig. 6).

The changes in plant-available moisture are less spatially coherent that the changes in temperature (Fig. 5). There is an increase in $\alpha_{plant,corrected}$ in some regions characterised by warming, for example, southeastern China and Japan; but there are mixed signals of drying and wetting in other re-

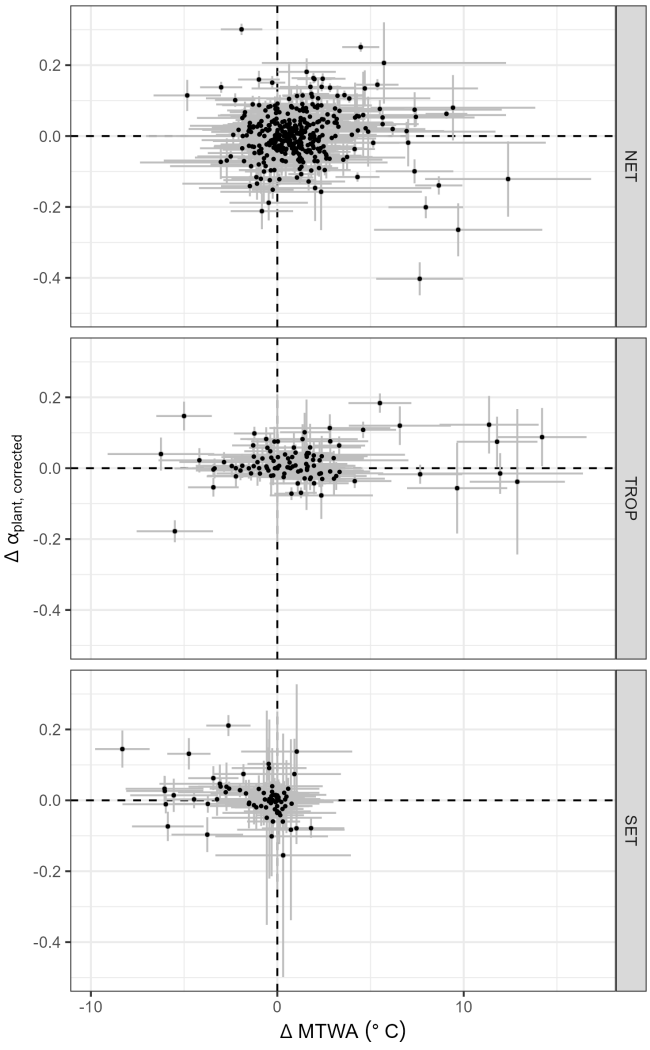

Figure 4. Scatter plot of the change in CO_2-corrected plant-available moisture ($\Delta\alpha_{plant,corrected}$) versus the change in mean temperature of the warmest month (ΔMTWA) during individual Dansgaard–Oeschger (D–O) events at individual sites. The points are grouped into the northern extratropics (NET, north of 23.5° N), the tropics (TROP, between 23.5° N and 23.5° S) and the southern extratropics (SET, south of 23.5° S). The grey lines indicate ±1 error of the change.

gions characterised by warming, such as southern Europe. Furthermore, regions characterised by cooling, such as western North America and the southern extratropics, can also show both drying and wetting. Changes in $\Delta\alpha_{plant,corrected}$ also show more variability between D–O events than changes in temperature (Fig. S7d). We have applied a correction for low CO_2 values during the glacial period to plant-available moisture. The actual values ($\alpha_{plant,corrected}$) are generally higher than the vegetation-based reconstructed values (α_{plant}) (Fig. S2a). However, the correction does not have a significant impact on the spatial patterns during D–O events (Figs. S2b and S7c).

4 Discussion and Conclusions

4.1 Comparison with previous reconstructions

We have presented a first attempt to map the spatial patterns of quantitative changes in seasonal temperatures and plant-available moisture during D–O events globally, using a consistent methodology. These analyses show that there is an anti-phasing between changes in the northern extratropics and the southern extratropics, with warming in the north and cooling in the south. The largest and most consistent warming during D–O events occurs in Eurasia. There is a significant difference between winter warming and summer warming in the northern extratropics, resulting in an overall reduction in seasonality. Site-based reconstructions from the Eifel region in central Europe, based on branched glycerol dialkyl glycerol tetraethers, indicate minimal temperature changes during summer (Zander et al., 2024) and thus support the idea that the D–O changes were driven by large changes in winter temperature. Zumaque et al., (2025) provide seasonal temperature and precipitation reconstructions for 12 of the sites from southern Europe (which are included in our fossil pollen records) but using the modern analogue technique as the reconstruction method and the Eurasian Modern Pollen Database version 2 (Davis et al., 2020) (EMPDv2; also included in SMPDSv3) as the modern training dataset. They show relatively stable summer temperatures but large change in MTCO through the MIS3 D–O events, consistent with our reconstructions (using a regression-based reconstruction method and a global modern training dataset) of a reduction in seasonality during warming events in the northern extratropics. We find no significant reduction in seasonality in the southern extratropics. Since only quantitative reconstructions of MAT (rather than MTCO and MTWA) are available from the southern extratropics (e.g. Fletcher and Thomas, 2010; Newnham et al., 2017), there is no independent confirmation of this result.

Qualitative interpretation of palaeo-records suggest that many regions are characterised by both warming and wetting, such as western Europe (Fletcher et al., 2010; Sánchez Goñi et al., 2008), eastern Europe (Fleitmann et al., 2009; Stockhecke et al., 2016), central Siberia (Grygar et al., 2006), and the Great Basin USA (Denniston et al., 2007; Jiménez-Moreno et al., 2010). Previous studies have also indicated drier conditions during D–O events, particularly in parts of the USA such as the Pacific Northwest (Grigg and Whitlock, 2002) and Florida (Grimm et al., 2006; Jiménez-Moreno et al., 2010). Our reconstructions show more mixed signals and that there is no globally consistent relationship between changes in temperature and moisture, either in regions characterised by warming or by cooling (Figs. 4 and 5).

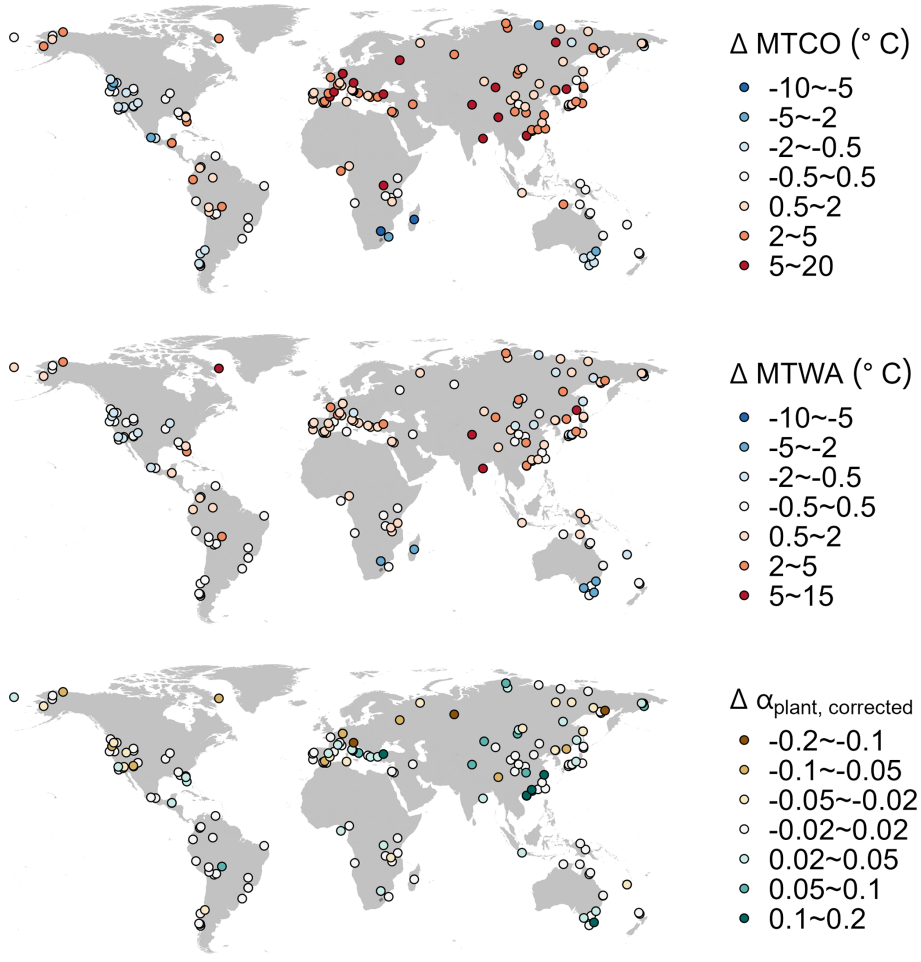

Figure 5. Map showing the median change of site-based reconstructions for Dansgaard–Oeschger (D–O) events 5 to 12. The panels from top to bottom show the changes in mean temperature of the coldest month (ΔMTCO), mean temperature of the warmest month (ΔMTWA) and CO_2-corrected plant-available moisture ($\Delta\alpha_{plant,corrected}$).

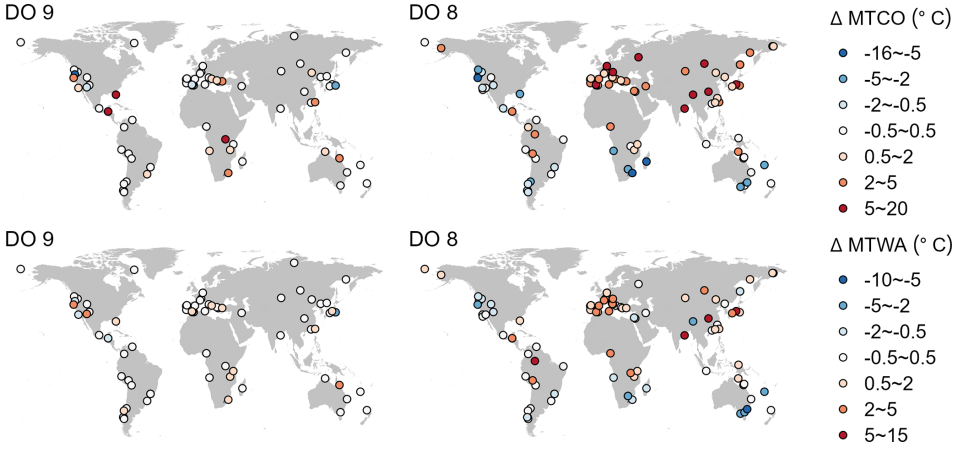

Figure 6. Map showing the change in mean temperature of the coldest month (ΔMTCO) and the change in mean temperature of the warmest month (ΔMTWA) for D–O 9 (a weak event) and D–O 8 (a strong event). The upper panel shows ΔMTCO, while the lower panel shows ΔMTWA.

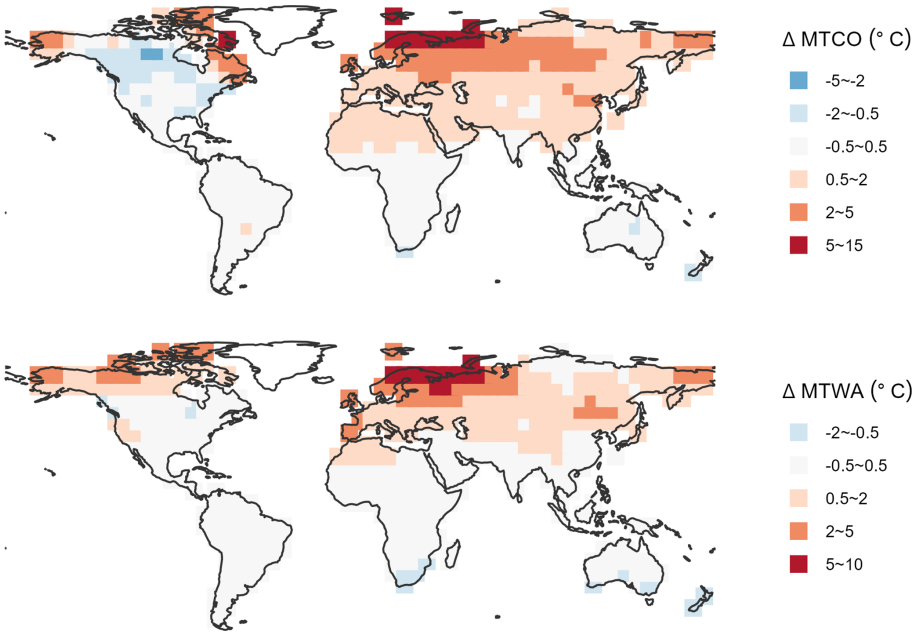

Figure 7. Map showing the median change of LOVECLIM simulations over (ice-free) land for Dansgaard–Oeschger (D–O) events 5 to 12. The upper panel shows the change in mean temperature of the coldest month (ΔMTCO), and the lower panel shows the change in mean temperature of the warmest month (ΔMTWA).

4.2 Global training dataset vs. local training dataset

We have used a global pollen dataset for calibration of the pollen-climate relationships. In general, reconstructions of glacial climates have used region-specific data sets (e.g. Dugerdil et al., 2021, 2025; Newnham et al., 2017; Wei et al., 2021; Zumaque et al., 2025). Herzschuh et al. (2023) made this explicit in their reconstructions of northern hemisphere climate over the past 30 000 years, by restricting the modern training data to within a 2000 km radius of individual fossil sites. The use of a region-specific raining data set can be justified on the grounds that it produces better statistics for the modern-day relationship between pollen abundance and specific climate variables. Nevertheless, as pointed out by Chevalier et al. (2020), an important issue is that the modern calibration data set has a span that adequately samples the climate space experienced in the past. The use of a global dataset for calibration makes it possible to sample a larger range of climates, and specifically to reconstruct climates that might be very different from the modern range in that region. For example, reconstructions of past European climate (Fig. S8) based on region-specific training dataset would yield less extreme winter temperatures than reconstructed using the global training data set. Although the trend and spatial pattern might not be influenced greatly, the amplitude of change might be underestimated.

The use of a global dataset, rather than region-specific training data, relies on the principle of phylogenetic niche conservatism (Harvey and Pagel, 1991; Qian and Ricklefs, 2004; Wang et al., 2025), which states that traits tend to remain constant over time. This also applies to the climate niche (Crisp and Cook, 2012; Jiang et al., 2023; Peterson, 2011; Wiens et al., 2010; Wiens and Graham, 2005) as evidenced by disjunct distributions of taxa across different continents (Yin et al., 2021). Niche conservatism underpins the fact that the modern distribution of specific genera can be predicted using climate-pollen relationships developed from other regions (e.g. Huntley et al., 1989). However, the use of a global dataset can create issues because of inconsistencies in taxonomic resolution between regions. The necessity for treating all species of *Quercus* as a single taxon, despite the fact that evergreen and deciduous species may occupy distinct climate niches in some regions, is a consequence of this. However, we have shown (Supplement, Sect. S4) that this has little impact on our reconstructions – largely because the climatic distinction that would be conveyed through separating deciduous and evergreen *Quercus* is also registered by the presence of other taxa. Although the use of a global training dataset for climate reconstructions has not been a common practice, it addresses the need to ensure that the modern training data adequately represents past climate conditions and also facilitates making reconstructions for sites from regions with limited modern pollen data.

4.3 Targets for model evaluation

The reconstructions in this paper can be used as targets for model evaluation, specifically the two transient D–O experiments planned for the next phase of the Palaeoclimate Modelling Intercomparison (see Malmierca-Vallet et al., 2023 for the experimental protocol). The first of these experiments is a baseline simulation starting at 34 ka, a time with low obliquity, moderate MIS3 greenhouse gas values, and an intermediate ice sheet configuration, which appears to be most conducive to generating D–O like behaviour in climate models. The second experiment involves the addition of freshwater, to examine whether this is necessary to precondition a state conducive to generating D–O events. The anti-phasing in reconstructed temperature changes between the northern and southern hemispheres is a general feature of climate model experiments. Most models show larger warming in winter than in summer in the northern hemisphere (e.g. Flückiger et al., 2008; Izumi et al., 2023; Van Meerbeeck et al., 2011), which is also consistent with our reconstructions. However, the cooling in western North America during D–O warming events in our reconstructions is not a feature of all climate model simulations.

Models generally show an intensification of the northern hemisphere monsoons during D–O events (e.g. Izumi et al., 2023; Menviel et al., 2020), but there is less consistency about changes in plant-available moisture in the extratropics. Our reconstructions show an increase in $\alpha_{\text{plant,corrected}}$ in southeastern China and Japan (Fig. 5). Although $\alpha_{\text{plant,corrected}}$ is not a direct reflection of summer precipitation, these changes are consistent with enhanced northern hemisphere monsoons during D–O warming events, as shown by speleothem records from the Caribbean (Warken et al., 2019) and speleothem and pollen records from Asia (Fohlmeister et al., 2023; Wang et al., 2001; Zorzi et al., 2022). However, there is more spatial variability and mixed signals in our reconstructions.

The LOVECLIM model was used as a reference to adjust the age scale in the reconstructions using MAT, but this does not preclude comparison of the seasonal temperatures. Here we approximate the winter-season temperature as MTCO and summer-season temperature as MTWA, since monthly temperatures are not available (only seasonal temperatures are available) in LOVECLIM. The general spatial pattern of simulated changes in MTCO and MTWA (Fig. 7) is consistent with the reconstructions, with largest warming in Eurasia, and cooling in the southern extratropics. The simulated changes are strong during D–O 8 but weak during D–O 9 (Fig. S9a, b), again as shown by the reconstructions. However, there are important differences. For example, simulated changes generally have smaller amplitude than shown by the reconstructions, and the cooling over western North America is generally only in winter, while the reconstructions show cooling over this region in both seasons. The relationship between ΔMTCO and ΔMTWA is also different (Fig. 8; Table 5): the simulated ΔMTCO is shown to be significantly larger than ΔMTWA in the northern extratropics, but significantly smaller than ΔMTWA in the southern extratropics, a contrast that is not so marked in the reconstructions. This comparison illustrates the usefulness of the reconstructions for model evaluation and to investigate the mechanisms that may not be adequately captured by current models.

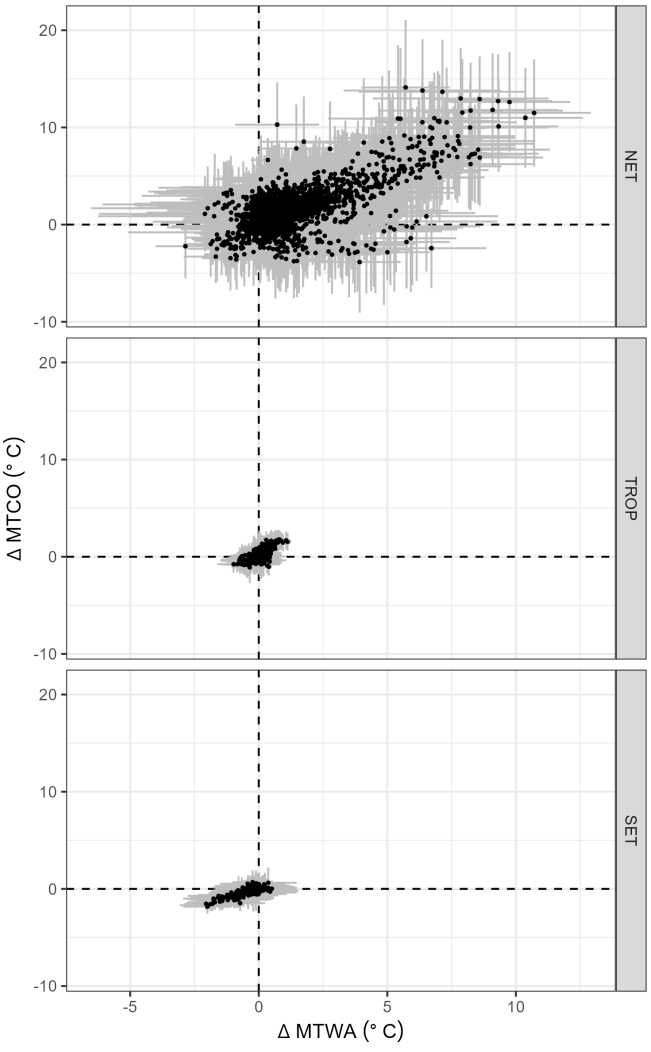

Figure 8. Scatter plot of the change in mean temperature of the coldest month (ΔMTCO) versus the change in mean temperature of the warmest month (ΔMTWA) during individual Dansgaard–Oeschger (D–O) events at individual (ice-free) land grids simulated by the LOVECLIM model, using the same way to identify changes as the reconstructions. The points are grouped into the northern extratropics (NET, north of 23.5° N), the tropics (TROP, between 23.5° N and 23.5° S) and the southern extratropics (SET, south of 23.5° S). The grey lines indicate ±1 error of the change.

Table 5. Maximum likelihood estimates of the relationship between the change in mean temperature of the coldest month (ΔMTCO) and the change in mean temperature of the warmest month (ΔMTWA) over (ice-free) land in LOVECLIM simulations, for the northern extratropics (NET, north of 23.5° N), tropics (TROP, between 23.5° N and 23.5° S) and southern extratropics (SET, south of 23.5° S). The intercepts were set to zero since both variables are changes.

Region		Coefficient	Standard error (SE)	Lower 95 %	Upper 95 %
NET	Slope	1.15	0.02	1.11	1.2
TROP	Slope	1.34	0.05	1.25	1.44
SET	Slope	0.76	0.03	0.70	0.81

4.4 Implications of the use of dynamic time warping

Identifying D–O events in pollen records is often problematic, particularly in regions where warming (especially if accompanied by dryer conditions) leads to a reduction (or an hiatus) in sedimentation as reflected in the variable resolution of the available pollen records (e.g. Camuera et al., 2022; Pini et al., 2022; Sinopoli et al., 2019; Wei et al., 2021). The use of dynamic time warping goes some way to improving the identification of potential D–O events. However, it precludes the calculation of a rate of change in climate. Thus, we have focused here on the magnitude of the changes during specific warming events. It is also likely that some of the variability in the reconstructed changes between different D–O events reflects imperfect identification of specific events because of the comparatively modest resolution of the records.

Code and data availability. The modern pollen dataset is available from https://doi.org/10.17864/1947.001473 (Harrison et al., 2025a). The original ACER database is available from Sánchez Goñi et al. (2017). The ACER2 fossil pollen data set is available from https://doi.org/10.17864/1947.001449 (Harrison et al., 2025b). Other data and codes used in this paper are available from https://doi.org/10.5281/zenodo.18218890 (Liu, 2026).

Supplement. The supplement related to this article is available online at https://doi.org/10.5194/cp-22-205-2026-supplement.

Author contributions. ML, SPH and ICP designed the study. ML made the reconstructions and produced the figures and tables. ML and SPH carried out the analyses. SPH wrote the first draft of the paper and all authors contributed to the final draft.

Competing interests. The contact author has declared that none of the authors has any competing interests.

Disclaimer. Publisher's note: Copernicus Publications remains neutral with regard to jurisdictional claims made in the text, published maps, institutional affiliations, or any other geographical representation in this paper. The authors bear the ultimate responsibility for providing appropriate place names. Views expressed in the text are those of the authors and do not necessarily reflect the views of the publisher.

Acknowledgements. ML acknowledges support from Imperial College through the Lee Family Scholarship. ICP acknowledges support from the ERC under the European Union Horizon 2020 research and innovation programme (grant agreement no.: 787203 REALM). SPH acknowledges fruitful discussions with colleagues from the D–O community working group. We would like to acknowledge our colleagues who provided original pollen data for inclusion in the ACER2 data set: Jon Camuera, Penelope González-Sampériz, Gonzalo Jiménez-Moreno, Xinghi Liu, Rewi Newnham, Jian Ni, Roberta Pini, Cassie Rowe, Frank Sirocco and María Del Socorro Lozano-García.

Financial support. This research has been supported by the FP7 Ideas: European Research Council (grant no. 787203 REALM) and Imperial College through the Lee Family Scholarship.

Review statement. This paper was edited by Odile Peyron and reviewed by Maria Fernanda Sanchez Goñi and two anonymous referees.

References

Abe-Ouchi, A., Segawa, T., and Saito, F.: Climatic Conditions for modelling the Northern Hemisphere ice sheets throughout the ice age cycle, Clim. Past, 3, 423–438, https://doi.org/10.5194/cp-3-423-2007, 2007.

Adolphi, F., Bronk Ramsey, C., Erhardt, T., Edwards, R. L., Cheng, H., Turney, C. S. M., Cooper, A., Svensson, A., Rasmussen, S. O., Fischer, H., and Muscheler, R.: Connecting the Greenland ice-core and U/Th timescales via cosmogenic radionuclides: testing the synchroneity of Dansgaard–Oeschger events, Clim. Past, 14, 1755–1781, https://doi.org/10.5194/cp-14-1755-2018, 2018.

Alshehri, M., Coenen, F., and Dures, K.: Effective sub-sequence-based dynamic time warping, in: Artificial Intelligence XXXVI, SGAI 2019, Lecture Notes in Computer Science, edited by: Bramer, M. and Petridis, M., Springer, Cham, p. 11927, https://doi.org/10.1007/978-3-030-34885-4_23, 2019.

Ampel, L., Bigler, C., Wohlfarth, B., Risberg, J., Lotter, A. F., and Veres, D.: Modest summer temperature variability during DO cycles in western Europe, Quat. Sci. Rev., 29, 1322–1327, https://doi.org/10.1016/j.quascirev.2010.03.002, 2010.

Bartlein, P. J., Harrison, S. P., Brewer, S., Connor, S., Davis, B. A. S., Gajewski, K., Guiot, J., Harrison-Prentice, T. I., Henderson, A., Peyron, O., Prentice, I. C., Scholze, M., Seppä, H., Shuman, B., Sugita, S., Thompson, R. S., Viau, A. E., Williams, J., and Wu, H.: Pollen-based continental climate reconstructions

at 6 and 21 ka: A global synthesis, Clim. Dyn., 37, 775–802, https://doi.org/10.1007/s00382-010-0904-1, 2011.

Bereiter, B., Eggleston, S., Schmitt, J., Nehrbass-Ahles, C., Stocker, T. F., Fischer, H., Kipfstuhl, S., and Chappellaz, J.: Revision of the EPICA Dome C CO_2 record from 800 to 600 kyr before present, Geophys. Res. Lett., 42, 542–549, https://doi.org/10.1002/2014GL061957, 2015.

Boucher-Lalonde, V., Morin, A., and Currie, D. J.: How are tree species distributed in climatic space? A simple and general pattern, Glob. Ecol. Biogeogr., 21, 1157–1166, https://doi.org/10.1111/j.1466-8238.2012.00764.x, 2012.

Burstyn, Y., Gazit, A., and Dvir, O.: Hierarchical dynamic time warping methodology for aggregating multiple geological time series, Comput. Geosci., 150, 104704, https://doi.org/10.1016/j.cageo.2021.104704, 2021.

Camuera, J., Ramos-Román, M. J., Jiménez-Moreno, G., García-Alix, A., Ilvonen, L., Ruha, L., Gil-Romera, G., González-Sampériz, P., and Seppä, H.: Past 200 kyr hydroclimate variability in the western Mediterranean and its connection to the African Humid Periods, Sci. Rep., 12, 9050, https://doi.org/10.1038/s41598-022-12047-1, 2022.

Cao, X., Tian, F., Andreev, A. A., Anderson, P. M., Lozhkin, A. V, Bezrukova, E. V, Ni, J., Rudaya, N., Stobbe, A., Wieczorek, M., and Herzschuh, U.: A taxonomically harmonized and temporally standardized fossil pollen dataset from Siberia covering the last 40 ka, PANGAEA [data set], https://doi.org/10.1594/PANGAEA.898616, 2019.

Cao, X., Tian, F., Andreev, A., Anderson, P. M., Lozhkin, A. V., Bezrukova, E., Ni, J., Rudaya, N., Stobbe, A., Wieczorek, M., and Herzschuh, U.: A taxonomically harmonized and temporally standardized fossil pollen dataset from Siberia covering the last 40 kyr, Earth Syst. Sci. Data, 12, 119–135, https://doi.org/10.5194/essd-12-119-2020, 2020.

Chevalier, M., Davis, B. A. S., Heiri, O., Seppä, H., Chase, B. M., Gajewski, K., Lacourse, T., Telford, R. J., Finsinger, W., Guiot, J., Kühl, N., Maezumi, S. Y., Tipton, J. R., Carter, V. A., Brussel, T., Phelps, L. N., Dawson, A., Zanon, M., Vallé, F., Nolan, C., Mauri, A., de Vernal, A., Izumi, K., Holmström, L., Marsicek, J., Goring, S., Sommer, P. S., Chaput, M., and Kupriyanov, D.: Pollen-based climate reconstruction techniques for late Quaternary studies, Earth-Science Rev., 210, 103384, https://doi.org/10.1016/j.earscirev.2020.103384, 2020.

Corrick, E. C., Drysdale, R. N., Hellstrom, J. C., Capron, E., Rasmussen, S. O., Zhang, X., Fleitmann, D., Couchoud, I., and Wolff, E.: Synchronous timing of abrupt climate changes during the last glacial period, Science, 369, 963–969, https://doi.org/10.1126/science.aay5538, 2020.

Crisp, M. D. and Cook, L. G.: Phylogenetic niche conservatism: What are the underlying evolutionary and ecological causes?, New Phytol., 196, 681–694, https://doi.org/10.1111/j.1469-8137.2012.04298.x, 2012.

Dansgaard, W., Johnsen, S. J., Clausen, H. B., Dahl-Jensen, D., Gundestrup, N. S., Hammer, C. U., Hvidberg, C. S., Steffensen, J. P., Sveinbjörnsdottir, A. E., Jouzel, J., and Bond, G.: Evidence for general instability of past climate from a 250-kyr ice-core record, Nature, 364, 218–220, https://doi.org/10.1038/364218a0, 1993.

Davis, B. A. S., Chevalier, M., Sommer, P., Carter, V. A., Finsinger, W., Mauri, A., Phelps, L. N., Zanon, M., Abegglen, R., Åkesson, C. M., Alba-Sánchez, F., Anderson, R. S., Antipina, T. G., Atanassova, J. R., Beer, R., Belyanina, N. I., Blyakharchuk, T. A., Borisova, O. K., Bozilova, E., Bukreeva, G., Bunting, M. J., Clò, E., Colombaroli, D., Combourieu-Nebout, N., Desprat, S., Di Rita, F., Djamali, M., Edwards, K. J., Fall, P. L., Feurdean, A., Fletcher, W., Florenzano, A., Furlanetto, G., Gaceur, E., Galimov, A. T., Gałka, M., García-Moreiras, I., Giesecke, T., Grindean, R., Guido, M. A., Gvozdeva, I. G., Herzschuh, U., Hjelle, K. L., Ivanov, S., Jahns, S., Jankovska, V., Jiménez-Moreno, G., Karpińska-Kołaczek, M., Kitaba, I., Kołaczek, P., Lapteva, E. G., Latałowa, M., Lebreton, V., Leroy, S., Leydet, M., Lopatina, D. A., López-Sáez, J. A., Lotter, A. F., Magri, D., Marinova, E., Matthias, I., Mavridou, A., Mercuri, A. M., Mesa-Fernández, J. M., Mikishin, Y. A., Milecka, K., Montanari, C., Morales-Molino, C., Mrotzek, A., Muñoz Sobrino, C., Naidina, O. D., Nakagawa, T., Nielsen, A. B., Novenko, E. Y., Panajiotidis, S., Panova, N. K., Papadopoulou, M., Pardoe, H. S., Pędziszewska, A., Petrenko, T. I., Ramos-Román, M. J., Ravazzi, C., Rösch, M., Ryabogina, N., Sabariego Ruiz, S., Salonen, J. S., Sapelko, T. V., Schofield, J. E., Seppä, H., Shumilovskikh, L., Stivrins, N., Stojakowits, P., Svobodova Svitavska, H., Święta-Musznicka, J., Tantau, I., Tinner, W., Tobolski, K., Tonkov, S., Tsakiridou, M., Valsecchi, V., Zanina, O. G., and Zimny, M.: The Eurasian Modern Pollen Database (EMPD), version 2, Earth Syst. Sci. Data, 12, 2423–2445, https://doi.org/10.5194/essd-12-2423-2020, 2020.

Davis, T. W., Prentice, I. C., Stocker, B. D., Thomas, R. T., Whitley, R. J., Wang, H., Evans, B. J., Gallego-Sala, A. V., Sykes, M. T., and Cramer, W.: Simple process-led algorithms for simulating habitats (SPLASH v.1.0): robust indices of radiation, evapotranspiration and plant-available moisture, Geosci. Model Dev., 10, 689–708, https://doi.org/10.5194/gmd-10-689-2017, 2017.

Denniston, R. F., Asmerom, Y., Polyak, V., Dorale, J. A., Carpenter, S. J., Trodick, C., Hoye, B., and Gonzaìlez, L. A.: Synchronous millennial-scale climatic changes in the Great Basin and the North Atlantic during the last interglacial, Geology, 35, 619–622, https://doi.org/10.1130/G23445A.1, 2007.

Dima, M., Lohmann, G., and Knorr, G.: North Atlantic versus global control on Dansgaard–Oeschger events, Geophys. Res. Lett., 45, 12991–12998, https://doi.org/10.1029/2018GL080035, 2018.

Doblas-Reyes, F. J., Sörensson, A. A., Almazroui, M., Dosio, A., Gutowski, W. J., Haarsma, R., Hamdi, R., Hewitson, B., Kwon, W.-T., Lamptey, B. L., Maraun, D., Stephenson, T. S., Takayabu, I., Terray, L., Turner, A., and Zuo, Z.: Linking global to regional climate change, in: Climate Change 2021 – The Physical Science Basis: Working Group I Contribution to the Sixth Assessment Report of the Intergovernmental Panel on Climate Change, edited by: Masson-Delmotte, V., Zhai, P., Pirani, A., Connors, S. L., Péan, C., Berger, S., Caud, N., Chen, Y., Goldfarb, L., Gomis, M. I., Huang, M., Leitzell, K., Lonnoy, E., Matthews, J. B. R., Maycock, T. K., Waterfield, T., Yelekçi, O., Yu, R., and Zhou, B., Cambridge University Press, Cambridge, United Kingdom and New York, NY, USA, 1363–1512, https://doi.org/10.1017/9781009157896.012, 2021.

Dugerdil, L., Joannin, S., Peyron, O., Jouffroy-Bapicot, I., Vannière, B., Boldgiv, B., Unkelbach, J., Behling, H., and Ménot, G.: Climate reconstructions based on GDGT and pollen surface datasets from Mongolia and Baikal area: calibrations and applicability to

extremely cold–dry environments over the Late Holocene, Clim. Past, 17, 1199–1226, https://doi.org/10.5194/cp-17-1199-2021, 2021.

Dugerdil, L., Peyron, O., Ménot, G., Egamberdieva, D., Alimov, J., Leroy, S. A. G., Garnier, E., Nowak, A., and Joannin, S.: First paleoenvironmental calibrations for modern pollen rain of Tajikistan and Uzbekistan: A case study of pollen – vegetation functional biogeography of Arid Central Asia, Glob. Planet. Change, 252, 104857, https://doi.org/10.1016/j.gloplacha.2025.104857, 2025.

Farquhar, G. D.: Carbon dioxide and vegetation, Science, 278, 1411, https://doi.org/10.1126/science.278.5342.1411, 1997.

Fleitmann, D., Cheng, H., Badertscher, S., Edwards, R. L., Mudelsee, M., Göktürk, O. M., Fankhauser, A., Pickering, R., Raible, C. C., Matter, A., Kramers, J., and Tüysüz, O.: Timing and climatic impact of Greenland interstadials recorded in stalagmites from northern Turkey, Geophys. Res. Lett., 36, https://doi.org/10.1029/2009GL040050, 2009.

Fletcher, M.-S. and Thomas, I.: A quantitative Late Quaternary temperature reconstruction from western Tasmania, Australia, Quat. Sci. Rev., 29, 2351–2361, https://doi.org/10.1016/j.quascirev.2010.06.012, 2010.

Fletcher, W. J., Sánchez Goñi, M. F., Allen, J. R. M., Cheddadi, R., Combourieu-Nebout, N., Huntley, B., Lawson, I., Londeix, L., Magri, D., Margari, V., Müller, U. C., Naughton, F., Novenko, E., Roucoux, K., and Tzedakis, P. C.: Millennial-scale variability during the last glacial in vegetation records from Europe, Quat. Sci. Rev., 29, 2839–2864, https://doi.org/10.1016/j.quascirev.2009.11.015, 2010.

Flückiger, J., Knutti, R., White, J. W. C., and Renssen, H.: Modeled seasonality of glacial abrupt climate events, Clim. Dyn., 31, 633–645, https://doi.org/10.1007/s00382-008-0373-y, 2008.

Fohlmeister, J., Sekhon, N., Columbu, A., Vettoretti, G., Weitzel, N., Rehfeld, K., Veiga-Pires, C., Ben-Yami, M., Marwan, N., and Boers, N.: Global reorganization of atmospheric circulation during Dansgaard–Oeschger cycles, Proc. Natl. Acad. Sci., 120, e2302283120, https://doi.org/10.1073/pnas.2302283120, 2023.

Garreta, V., Miller, P. A., Guiot, J., Hély, C., Brewer, S., Sykes, M. T., and Litt, T.: A method for climate and vegetation reconstruction through the inversion of a dynamic vegetation model, Clim. Dyn., 35, 371–389, https://doi.org/10.1007/s00382-009-0629-1, 2010.

Gerhart, L. M. and Ward, J. K.: Plant responses to low [CO_2] of the past, New Phytol., 188, 674–695, https://doi.org/10.1111/j.1469-8137.2010.03441.x, 2010.

Giorgino, T.: Computing and visualizing Dynamic Time Warping alignments in R: The dtw package, J. Stat. Softw., 31, 1–24, https://doi.org/10.18637/jss.v031.i07, 2009.

Grigg, L. D. and Whitlock, C.: Patterns and causes of millennial-scale climate change in the Pacific Northwest during Marine Isotope Stages 2 and 3, Quat. Sci. Rev., 21, 2067–2083, https://doi.org/10.1016/S0277-3791(02)00017-3, 2002.

Grimm, E. C., Watts, W. A., Jacobson, G. L., Hansen, B. C. S., Almquist, H. R., and Dieffenbacher-Krall, A. C.: Evidence for warm wet Heinrich events in Florida, Quat. Sci. Rev., 25, 2197–2211, https://doi.org/10.1016/j.quascirev.2006.04.008, 2006.

Grygar, T., Kadlec, J., Pruner, P., Swann, G., Bezdička, P., Hradil, D., Lang, K., Novotna, K., and Oberhänsli, H.: Paleoenvironmental record in Lake Baikal sediments: Environmental changes in the last 160 ky, Palaeogeogr. Palaeoclimatol. Palaeoecol., 237, 240–254, https://doi.org/10.1016/j.palaeo.2005.12.007, 2006.

Guiot, J., de Beaulieu, J. L., Cheddadi, R., David, F., Ponel, P., and Reille, M.: The climate in Western Europe during the last Glacial/Interglacial cycle derived from pollen and insect remains, Palaeogeogr. Palaeoclimatol. Palaeoecol., 103, 73–93, https://doi.org/10.1016/0031-0182(93)90053-L, 1993.

Guiot, J., Torre, F., Jolly, D., Peyron, O., Boreux, J. J., and Cheddadi, R.: Inverse vegetation modeling by Monte Carlo sampling to reconstruct palaeoclimates under changed precipitation seasonality and CO2 conditions: Application to glacial climate in Mediterranean region, Ecol. Modell., 127, 119–140, https://doi.org/10.1016/S0304-3800(99)00219-7, 2000.

Guiot, J., Wu, H. B., Garreta, V., Hatté, C., and Magny, M.: A few prospective ideas on climate reconstruction: from a statistical single proxy approach towards a multi-proxy and dynamical approach, Clim. Past, 5, 571–583, https://doi.org/10.5194/cp-5-571-2009, 2009.

Harris, I., Osborn, T. J., Jones, P., and Lister, D.: Version 4 of the CRU TS monthly high-resolution gridded multivariate climate dataset, Sci. Data, 7, 109, https://doi.org/10.1038/s41597-020-0453-3, 2020.

Harrison, S. P.: Climate reconstructions for the SMPDS v1 modern pollen data set, Univ. Read., Zenodo [data set], https://doi.org/10.5281/zenodo.3605003, 2020.

Harrison, S. P. and Sanchez Goñi, M. F.: Global patterns of vegetation response to millennial-scale variability and rapid climate change during the last glacial period, Quat. Sci. Rev., 29, 2957–2980, https://doi.org/10.1016/j.quascirev.2010.07.016, 2010.

Harrison, S., Egbudom, M.-A., and Villegas-Diaz, R.: The SPECIAL Modern Pollen Data Set for Climate Reconstructions, version 3 (SMPDSv3), University of Reading [data set], https://doi.org/10.17864/1947.001473, 2025a.

Harrison, S., Egbudom, M.-A., and Liu, M.: ACER2: The Abrupt Climate Changes and Environmental Responses Database (version 2), University of Reading [data set], https://doi.org/10.17864/1947.001449, 2025b.

Harrison, S. P., Bartlein, P. J., Cruz-Silva, E., Haas, O., Jackson, S. T., Kaushal, N., Liu, M., Magri, D., Robson, D., Vettoretti, G., and Prentice, I. C.: Palaeoclimate perspectives on contemporary climate change, Ann. Rev. Environ. Resour., 50, https://doi.org/10.1146/annurev-environ-112922-110121, 2025c.

Harvey, P. H. and Pagel, M. D.: The comparative method in evolutionary biology, Oxford University Press, https://doi.org/10.1093/oso/9780198546412.001.0001, 1991.

Hatfield, J. L. and Dold, C.: Water-use efficiency: Advances and challenges in a changing climate, Front. Plant Sci., 10, https://doi.org/10.3389/fpls.2019.00103, 2019.

Herzschuh, U., Böhmer, T., Li, C., Chevalier, M., Hébert, R., Dallmeyer, A., Cao, X., Bigelow, N. H., Nazarova, L., Novenko, E. Y., Park, J., Peyron, O., Rudaya, N. A., Schlütz, F., Shumilovskikh, L. S., Tarasov, P. E., Wang, Y., Wen, R., Xu, Q., and Zheng, Z.: LegacyClimate 1.0: a dataset of pollen-based climate reconstructions from 2594 Northern Hemisphere sites covering the last 30 kyr and beyond, Earth Syst. Sci. Data, 15, 2235–2258, https://doi.org/10.5194/essd-15-2235-2023, 2023.

Huber, C., Leuenberger, M., Spahni, R., Flückiger, J., Schwander, J., Stocker, T. F., Johnsen, S., Landais, A., and Jouzel, J.: Iso-

tope calibrated Greenland temperature record over Marine Isotope Stage 3 and its relation to CH_4, Earth Planet. Sci. Lett., 243, 504–519, https://doi.org/10.1016/j.epsl.2006.01.002, 2006.

Huntley, B., Bartlein, P. J., and Prentice, I. C.: Climatic control of the distribution and abundance of Beech (Fagus L.) in Europe and North America, J. Biogeogr., 16, 551–560, https://doi.org/10.2307/2845210, 1989.

Huntley, B., Watts, W. A., Allen, J. R. M., and Zolitschka, B.: Palaeoclimate, chronology and vegetation history of the Weichselian Lateglacial: comparative analysis of data from three cores at Lago Grande di Monticchio, southern Italy, Quat. Sci. Rev., 18, 945–960, https://doi.org/10.1016/S0277-3791(99)00007-4, 1999.

IPCC: Climate change 2022: Impacts, adaptation and vulnerability. Contribution of working group II to the sixth assessment report of the Intergovernmental Panel on Climate Change, edited by: Pörtner, H.-O., Roberts, D. C., Tignor, M., Poloczanska, E. S., Mintenbeck, K., Alegría, A., Craig, M., Langsdorf, S., Löschke, S., Möller, V., Okem, A., and Rama, B., Cambridge University Press, Cambridge University Press, Cambridge, UK and New York, NY, USA, https://doi.org/10.1017/9781009325844, 2022.

Izumi, K. and Bartlein, P. J.: North American paleoclimate reconstructions for the Last Glacial Maximum using an inverse modeling through iterative forward modeling approach applied to pollen data, Geophys. Res. Lett., 43, 10965–10972, https://doi.org/10.1002/2016GL070152, 2016.

Izumi, K., Armstrong, E., and Valdes, P.: Global footprints of dansgaard-oeschger oscillations in a GCM, Quat. Sci. Rev., 305, 108016, https://doi.org/10.1016/j.quascirev.2023.108016, 2023.

Jiang, K., Wang, Q., Dimitrov, D., Luo, A., Xu, X., Su, X., Liu, Y., Li, Y., Li, Y., and Wang, Z.: Evolutionary history and global angiosperm species richness–climate relationships, Glob. Ecol. Biogeogr., 32, 1059–1072, https://doi.org/10.1111/geb.13687, 2023.

Jiménez-Moreno, G., Anderson, R. S., Desprat, S., Grigg, L. D., Grimm, E. C., Heusser, L. E., Jacobs, B. F., López-Martínez, C., Whitlock, C. L., and Willard, D. A.: Millennial-scale variability during the last glacial in vegetation records from North America, Quat. Sci. Rev., 29, 2865–2881, https://doi.org/10.1016/j.quascirev.2009.12.013, 2010.

Kindler, P., Guillevic, M., Baumgartner, M., Schwander, J., Landais, A., and Leuenberger, M.: Temperature reconstruction from 10 to 120 kyr b2k from the NGRIP ice core, Clim. Past, 10, 887–902, https://doi.org/10.5194/cp-10-887-2014, 2014.

Lapellegerie, P., Millet, L., Rius, D., Duprat-Oualid, F., Luoto, T., and Heiri, O.: Chironomid-inferred summer temperature during the Last Glacial Maximum in the Southern Black Forest, Central Europe, Quat. Sci. Rev., 345, 109016, https://doi.org/10.1016/j.quascirev.2024.109016, 2024.

Lee, J.-Y., Marotzke, J., Bala, G., Cao, L., Corti, S., Dunne, J. P., Engelbrecht, F., Fischer, E., Fyfe, J. C., Jones, C., Maycock, A., Mutemi, J., Ndiaye, O., Panickal, S., and Zhou, T.: Future global climate: Scenario-based projections and near-term information, in Climate change 2021: The physical science basis. Contribution of working group I to the sixth assessment report of the Intergovernmental Panel on Climate Change, edited by: Masson-Delmotte, V., Zhai, P., Pirani, A., Connors, S. L., Péan, C., Berger, S., Caud, N., Chen, Y., Goldfarb, L., Gomis, M. I., Huang, M., Leitzell, K., Lonnoy, E., Matthews, J. B. R., Maycock, T. K., Waterfield, T., Yelekçi, O., Yu, R., and Zhou, B., Cambridge University Press, Cambridge, United Kingdom and New York, NY, USA, 553–672, https://doi.org/10.1017/9781009157896.006, 2021.

Li, C., Ni, J., Böhmer, T., Cao, X., Zhou, B., Liao, M., Li, K., Schild, L., Wieczorek, M., Heim, B., and Herzschuh, U.: LegacyPollen2.0: an updated global taxonomically and temporally standardized fossil pollen dataset of 3680 palynological records, PANGAEA [data set], https://doi.org/10.1594/PANGAEA.965907, 2025.

Liu, M.: DO climate reconstruction, Zenodo [data set and code], https://doi.org/10.5281/zenodo.18218890, 2026.

Liu, M., Prentice, I. C., ter Braak, C. J. F., and Harrison, S. P.: An improved statistical approach for reconstructing past climates from biotic assemblages, Proc. R. Soc. A Math., 476, 20200346, https://doi.org/10.1098/rspa.2020.0346, 2020.

Liu, M., Prentice, I. C., Menviel, L., and Harrison, S. P.: Past rapid warmings as a constraint on greenhouse-gas climate feedbacks, Commun. Earth Environ., 3, 196, https://doi.org/10.1038/s43247-022-00536-0, 2022.

Liu, M., Shen, Y., González-Sampériz, P., Gil-Romera, G., ter Braak, C. J. F., Prentice, I. C., and Harrison, S. P.: Holocene climates of the Iberian Peninsula: pollen-based reconstructions of changes in the west–east gradient of temperature and moisture, Clim. Past, 19, 803–834, https://doi.org/10.5194/cp-19-803-2023, 2023.

Malmierca-Vallet, I., Sime, L. C., and the D–O community members: Dansgaard–Oeschger events in climate models: review and baseline Marine Isotope Stage 3 (MIS3) protocol, Clim. Past, 19, 915–942, https://doi.org/10.5194/cp-19-915-2023, 2023.

Martrat, B., Grimalt, J. O., Shackleton, N. J., de Abreu, L., Hutterli, M. A., and Stocker, T. F.: Four climate cycles of recurring deep and surface water destabilizations on the Iberian margin, Science, 317, 502–507, https://doi.org/10.1126/science.1139994, 2007.

Menviel, L., Timmermann, A., Friedrich, T., and England, M. H.: Hindcasting the continuum of Dansgaard–Oeschger variability: mechanisms, patterns and timing, Clim. Past, 10, 63–77, https://doi.org/10.5194/cp-10-63-2014, 2014.

Menviel, L., Skinner, L. C., Tarasov, L., and Tzedakis, P. C.: An ice–climate oscillatory framework for Dansgaard–Oeschger cycles, Nat. Rev. Earth Environ., 1, 677–693, https://doi.org/10.1038/s43017-020-00106-y, 2020.

Newnham, R. M., Alloway, B. V, Holt, K. A., Butler, K., Rees, A. B. H., Wilmshurst, J. M., Dunbar, G., and Hajdas, I.: Last Glacial pollen–climate reconstructions from Northland, New Zealand, J. Quat. Sci., 32, 685–703, https://doi.org/10.1002/jqs.2955, 2017.

Peterson, A. T.: Ecological niche conservatism: A time-structured review of evidence, J. Biogeogr., 38, 817–827, https://doi.org/10.1111/j.1365-2699.2010.02456.x, 2011.

Pini, R., Furlanetto, G., Vallé, F., Badino, F., Wick, L., Anselmetti, F. S., Bertuletti, P., Fusi, N., Morlock, M. A., Delmonte, B., Harrison, S. P., Maggi, V., and Ravazzi, C.: Linking North Atlantic and Alpine Last Glacial Maximum climates via a high-resolution pollen-based subarctic forest steppe record, Quat. Sci. Rev., 294, 107759, https://doi.org/10.1016/j.quascirev.2022.107759, 2022.

Prentice, I. C. and Harrison, S. P.: Ecosystem effects of CO_2 concentration: evidence from past climates, Clim. Past, 5, 297–307, https://doi.org/10.5194/cp-5-297-2009, 2009.

Prentice, I. C., Cleator, S. F., Huang, Y. H., Harrison, S. P., and Roulstone, I.: Reconstructing ice-age palaeoclimates: Quantifying low-CO_2 effects on plants, Glob. Planet. Change, 149, 166–176, https://doi.org/10.1016/j.gloplacha.2016.12.012, 2017.

Prentice, I. C., Villegas-Diaz, R., and Harrison, S. P.: Accounting for atmospheric carbon dioxide variations in pollen-based reconstruction of past hydroclimates, Glob. Planet. Change, 211, 103790, https://doi.org/10.1016/j.gloplacha.2022.103790, 2022a.

Prentice, I. C., Villegas-Diaz, R., and Harrison, S. P.: codos: CO_2 correction tools, Zenodo [code], https://doi.org/10.5281/zenodo.5083309, 2022b.

Prud'homme, C., Fischer, P., Jöris, O., Gromov, S., Vinnepand, M., Hatté, C., Vonhof, H., Moine, O., Vött, A., and Fitzsimmons, K. E.: Millennial-timescale quantitative estimates of climate dynamics in central Europe from earthworm calcite granules in loess deposits, Commun. Earth Environ., 3, 267, https://doi.org/10.1038/s43247-022-00595-3, 2022.

Qian, H. and Ricklefs, R. E.: Geographical distribution and ecological conservatism of disjunct genera of vascular plants in eastern Asia and eastern North America, J. Ecol., 92, 253–265, https://doi.org/10.1111/j.0022-0477.2004.00868.x, 2004.

Sánchez Goñi, M., Cacho, I., Turon, J., Guiot, J., Sierro, F., Peypouquet, J., Grimalt, J., and Shackleton, N.: Synchroneity between marine and terrestrial responses to millennial scale climatic variability during the last glacial period in the Mediterranean region, Clim. Dyn., 19, 95–105, https://doi.org/10.1007/s00382-001-0212-x, 2002.

Sánchez Goñi, M. F., Landais, A., Fletcher, W. J., Naughton, F., Desprat, S., and Duprat, J.: Contrasting impacts of Dansgaard–Oeschger events over a western European latitudinal transect modulated by orbital parameters, Quat. Sci. Rev., 27, 1136–1151, https://doi.org/10.1016/j.quascirev.2008.03.003, 2008.

Sánchez Goñi, M. F., Desprat, S., Daniau, A.-L., Bassinot, F. C., Polanco-Martínez, J. M., Harrison, S. P., Allen, J. R. M., Anderson, R. S., Behling, H., Bonnefille, R., Burjachs, F., Carrión, J. S., Cheddadi, R., Clark, J. S., Combourieu-Nebout, N., Mustaphi, Colin. J. Courtney, Debusk, G. H., Dupont, L. M., Finch, J. M., Fletcher, W. J., Giardini, M., González, C., Gosling, W. D., Grigg, L. D., Grimm, E. C., Hayashi, R., Helmens, K., Heusser, L. E., Hill, T., Hope, G., Huntley, B., Igarashi, Y., Irino, T., Jacobs, B., Jiménez-Moreno, G., Kawai, S., Kershaw, A. P., Kumon, F., Lawson, I. T., Ledru, M.-P., Lézine, A.-M., Liew, P. M., Magri, D., Marchant, R., Margari, V., Mayle, F. E., McKenzie, G. M., Moss, P., Müller, S., Müller, U. C., Naughton, F., Newnham, R. M., Oba, T., Pérez-Obiol, R., Pini, R., Ravazzi, C., Roucoux, K. H., Rucina, S. M., Scott, L., Takahara, H., Tzedakis, P. C., Urrego, D. H., van Geel, B., Valencia, B. G., Vandergoes, M. J., Vincens, A., Whitlock, C. L., Willard, D. A., and Yamamoto, M.: The ACER pollen and charcoal database: a global resource to document vegetation and fire response to abrupt climate changes during the last glacial period, Earth Syst. Sci. Data, 9, 679–695, https://doi.org/10.5194/essd-9-679-2017, 2017.

Sinopoli, G., Peyron, O., Masi, A., Holtvoeth, J., Francke, A., Wagner, B., and Sadori, L.: Pollen-based temperature and precipitation changes in the Ohrid Basin (western Balkans) between 160 and 70 ka, Clim. Past, 15, 53–71, https://doi.org/10.5194/cp-15-53-2019, 2019.

Stockhecke, M., Timmermann, A., Kipfer, R., Haug, G. H., Kwiecien, O., Friedrich, T., Menviel, L., Litt, T., Pickarski, N., and Anselmetti, F. S.: Millennial to orbital-scale variations of drought intensity in the Eastern Mediterranean, Quat. Sci. Rev., 133, 77–95, https://doi.org/10.1016/j.quascirev.2015.12.016, 2016.

Timm, O., Timmermann, A., Abe-Ouchi, A., Saito, F., and Segawa, T.: On the definition of seasons in paleoclimate simulations with orbital forcing, Paleoceanography, 23, https://doi.org/10.1029/2007PA001461, 2008.

Turner, M. G., Wei, D., Prentice, I. C., and Harrison, S. P.: The impact of methodological decisions on climate reconstructions using WA-PLS, Quat. Res., 99, 341–356, https://doi.org/10.1017/qua.2020.44, 2020.

Újvári, G., Bernasconi, S. M., Stevens, T., Kele, S., Páll-Gergely, B., Surányi, G., and Demény, A.: Stadial-interstadial temperature and aridity variations in east central Europe preceding the Last Glacial Maximum, Paleoceanogr. Paleoclimatology, 36, e2020PA004170, https://doi.org/10.1029/2020PA004170, 2021.

Van Meerbeeck, C. J., Renssen, H., Roche, D. M., Wohlfarth, B., Bohncke, S. J. P., Bos, J. A. A., Engels, S., Helmens, K. F., Sánchez-Goñi, M. F., Svensson, A., and Vandenberghe, J.: The nature of MIS 3 stadial–interstadial transitions in Europe: New insights from model–data comparisons, Quat. Sci. Rev., 30, 3618–3637, https://doi.org/10.1016/j.quascirev.2011.08.002, 2011.

Veres, D., Bazin, L., Landais, A., Toyé Mahamadou Kele, H., Lemieux-Dudon, B., Parrenin, F., Martinerie, P., Blayo, E., Blunier, T., Capron, E., Chappellaz, J., Rasmussen, S. O., Severi, M., Svensson, A., Vinther, B., and Wolff, E. W.: The Antarctic ice core chronology (AICC2012): an optimized multi-parameter and multi-site dating approach for the last 120 thousand years, Clim. Past, 9, 1733–1748, https://doi.org/10.5194/cp-9-1733-2013, 2013.

Vettoretti, G. and Peltier, W. R.: Interhemispheric air temperature phase relationships in the nonlinear Dansgaard–Oeschger oscillation, Geophys. Res. Lett., 42, 1180–1189, https://doi.org/10.1002/2014GL062898, 2015.

Voelker, A. H. L.: Global distribution of centennial-scale records for Marine Isotope Stage (MIS) 3: a database, Quat. Sci. Rev., 21, 1185–1212, https://doi.org/10.1016/S0277-3791(01)00139-1, 2002.

Wang, C., Wang, M., Zhu, S., Wu, X., Yang, S., Yan, Y., and Wen, Y.: Multiple ecological niche modeling reveals niche conservatism and divergence in East Asian Yew (Taxus), Plants, 14, https://doi.org/10.3390/plants14071094, 2025.

Wang, H., Prentice, I. C., and Ni, J.: Data-based modelling and environmental sensitivity of vegetation in China, Biogeosciences, 10, 5817–5830, https://doi.org/10.5194/bg-10-5817-2013, 2013.

Wang, Y. J., Cheng, H., Edwards, R. L., An, Z. S., Wu, J. Y., Shen, C.-C., and Dorale, J. A.: A high-resolution absolute-dated Late Pleistocene monsoon record from Hulu Cave, China, Science, 294, 2345–2348, https://doi.org/10.1126/science.1064618, 2001.

Warken, S. F., Scholz, D., Spötl, C., Jochum, K. P., Pajón, J. M., Bahr, A., and Mangini, A.: Caribbean hydroclimate and vegetation history across the last glacial period, Quat. Sci. Rev., 218, 75–90, https://doi.org/10.1016/j.quascirev.2019.06.019, 2019.

Wei, D., Prentice, I. C., and Harrison, S. P.: The climatic space of European pollen taxa, Ecology, 101, e03055, https://doi.org/10.1002/ecy.3055, 2020.

Wei, D., González-Sampériz, P., Gil-Romera, G., Harrison, S. P., and Prentice, I. C.: Seasonal temperature and moisture changes in interior semi-arid Spain from the last interglacial to the Late Holocene, Quat. Res., 101, 143–155, https://doi.org/10.1017/qua.2020.108, 2021.

Wiens, J. and Graham, C.: Niche conservatism: Integrating evolution, ecology, and conservation biology, Annu. Rev. Ecol. Evol. Syst., 36, 519–539, https://doi.org/10.1146/annurev.ecolsys.36.102803.095431, 2005.

Wiens, J., Ackerly, D., Allen, A., Anacker, B., Buckley, L., Cornell, H., Damschen, E., Davies, J., Grytnes, J. A., Harrison, S., Hawkins, B., Holt, R., Mccain, C., and Stephens, P.: Niche conservatism as an emerging principle in ecology and conservation biology, Ecol. Lett., 13, 1310–1324, https://doi.org/10.1111/j.1461-0248.2010.01515.x, 2010.

Wolff, E. W., Chappellaz, J., Blunier, T., Rasmussen, S. O., and Svensson, A.: Millennial-scale variability during the last glacial: The ice core record, Quat. Sci. Rev., 29, 2828–2838, https://doi.org/10.1016/j.quascirev.2009.10.013, 2010.

Woodward, F. I.: Climate and Plant Distribution, Cambridge University Press, Cambridge, UK, ISBN 0-521-23766-1, 1987.

Wu, H., Guiot, J., Brewer, S., and Guo, Z.: Climatic changes in Eurasia and Africa at the last glacial maximum and mid-Holocene: Reconstruction from pollen data using inverse vegetation modelling, Clim. Dyn., 29, 211–229, https://doi.org/10.1007/s00382-007-0231-3, 2007.

Yin, X., Jarvie, S., Guo, W.-Y., Deng, T., Mao, L., Zhang, M., Chu, C., Qian, H., Svenning, J.-C., and He, F.: Niche overlap and divergence times support niche conservatism in eastern Asia–eastern North America disjunct plants, Glob. Ecol. Biogeogr., 30, 1990–2003, https://doi.org/10.1111/geb.13360, 2021.

Zander, P. D., Böhl, D., Sirocko, F., Auderset, A., Haug, G. H., and Martínez-García, A.: Reconstruction of warm-season temperatures in central Europe during the past 60 000 years from lacustrine branched glycerol dialkyl glycerol tetraethers (brGDGTs), Clim. Past, 20, 841–864, https://doi.org/10.5194/cp-20-841-2024, 2024.

Zhou, B.-R., Liao, M.-N., Li, K., Xu, D.-Y., Chen, H.-Y., Ni, J., Cao, X.-Y., Kong, Z.-C., Xu, Q.-H., Zhang, Y., Herzschuh, U., Cai, Y.-L., Chen, B.-S., Chen, J.-A., Chen, L.-K., Cheng, B., Gao, Y., Huang, X.-Z., Li, S.-F., Li, W.-Y., Liu, K.-B., Liu, G.-X., Liu, P.-M., Liu, X.-Q., Ma, C.-M., Song, C.-Q., Sun, X.-J., Tang, L.-Y., Wang, M.-H., Wang, Y.-B., Xu, J.-S., Yan, S., Yang, X.-D., Yao, Y.-F., Ye, C.-Y., Zhang, Z.-Y., Zhao, Z.-Y., Zheng, Z., and Zhu, C.: A fossil pollen dataset of China, Chinese J. Plant Ecol., 47, 1453–1463, https://www.plant-ecology.com (last access: 25 January 2026), 2023.

Zorzi, C., Desprat, S., Clément, C., Thirumalai, K., Oliviera, D., Anupama, K., Prasad, S., and Martinez, P.: When eastern India oscillated between desert versus savannah-dominated vegetation, Geophys. Res. Lett., 49, e2022GL099417, https://doi.org/10.1029/2022GL099417, 2022.

Zumaque, J., de Vernal, A., Fréchette, B., Guiot, J., Sánchez-Goñi, M. F., Barhoumi, C., Peyron, O., Peros, M., Burke, A., Camuera, J., Jiménez-Moreno, G., and Ramos-Román, M. J.: Decoupled winter and summer climate changes in southern Europe during the Dansgaard–Oeschger cycles, Quat. Sci. Rev., 359, 109273, https://doi.org/10.1016/j.quascirev.2025.109273, 2025.